Determining gas transfer velocities and CO_2 evasion fluxes from streams using carbon dioxide as a tracer

by

Mollie Jean McDowell

B.A. (Cum Laude), Amherst College, 2014

A THESIS SUBMITTED IN PARTIAL FULFILLMENT OF

THE REQUIREMENTS FOR THE DEGREE OF

MASTER OF SCIENCE

in

THE FACULTY OF GRADUATE AND POSTDOCTORAL

STUDIES

(Geological Sciences)

THE UNIVERSITY OF BRITISH COLUMBIA

(Vancouver)

August 2017

Abstract

Evasion of carbon dioxide (CO_2) from headwater streams is a dominant process controlling the fate of terrestrially-derived carbon (C) in inland waters. However, methodological limitations associated with determining the gas transfer velocity of carbon dioxide (k_{CO2}) in headwater streams inhibit efforts to accurately quantify CO_2 emissions. In this thesis, I present a proof of concept for a tracer gas method that mitigates common issues associated with conventional methods for determining k_{CO2}. In this method, a datalogger controls *in situ* stream sensors that measure the partial pressure of CO_2 (pCO_2) and other stream parameters as well as a solenoid valve connected to a compressed CO_2 cylinder. Automated injections of CO_2 were made via an aquatic diffuser located on the stream bed. Infrared gas-analyzing (IRGA) CO_2-type sensors enclosed in waterproof, gas-permeable membranes located downstream from the diffuser continuously measured aqueous pCO_2 and equilibrate to elevated values during CO_2 injections. The difference between upstream and downstream pCO_2 values during CO_2 injection relative to pre-injection concentrations permitted calculation of both the CO_2 flux from the reach and k_{CO2}. This method improves upon conventional methods due to its automation, *in situ* measurement, and use of CO_2 as a tracer rather than another gas, thereby reducing analytical error and increasing the frequency and timing with which measurements can be made relative to conventional methods. I tested this method in a headwater stream in southwestern British Columbia. I calculated k_{CO2} and continuous CO_2 emissions from the reach and compared both datasets to hydrogeomorphic parameters as well as values in the literature. Values of k_{CO2} were generally above the average values reported in the literature, but they corresponded well to values reported for steep, turbulent headwater streams. Values of k_{CO2} varied in relation to discharge, flow velocity, and stream temperature. CO_2 emissions from the stream were highest

during high flow events. Headwater streams, which have been shown to be "hotspots" for CO_2 emissions, can also be considered as exhibiting "hot moments" of CO_2 evasion.

Lay summary

Characterizing the global carbon cycle is important for many aspects of earth science, including those associated with climate change. Inland waters, such as streams, rivers, lakes, and estuaries, play a role in the carbon cycle by carrying carbon from the land into the ocean. Researchers have recently discovered that inland waters, and headwater streams in particular, do not just carry carbon but also process it, such that much of the carbon that enters an inland water body is either stored in sediments or evades into the atmosphere as carbon dioxide (CO_2), a potent greenhouse gas. However, limitations of current methods for measuring CO_2 evasion from streams have resulted in analytical errors and a dearth of data. In this thesis, I outline a new method that mitigates many of the errors associated with conventional methods for determining CO_2 evasion from streams.

Preface

This thesis was completed under the supervision of Dr. Mark S. Johnson, who provided the project idea, grant funding, guidance, suggestions, and editing assistance. Dr. R. Dan Moore also provided support as a supervisory committee member, particularly regarding hydrological measurements and statistical analyses. It is the original and unpublished work of the author, Mollie J. McDowell.

Table of Contents

List of tables

List of figures

List of symbols and acronyms

Symbol/Acronym	Units (constant)	Definition
Fr	N/A	Froude number
adj. r^2	N/A	coefficient of determination adjusted for number of external regressors
RSE	m d^{-1}	residual standard error
r^2	N/A	coefficient of determination
$k_H^{\ominus}$	atm M^{-1} (0.035)	Henry's Law constant for solubility in water at standard temperature and pressure
$T^{\ominus}$	K (298.15)	temperature at standard temperature and pressure
C	g	carbon
CO_2	N/A	carbon dioxide
$CO_{2(air)}$	μatm atm^{-1}	atmospheric pCO_2
$CO_{2(aq)}$	μatm atm^{-1}	stream pCO_2
d	m	depth/stage
F	g L^{-1} d^{-1}	flux
F_{CO2}	g C L^{-1} d^{-1}	flux of carbon dioxide
IRGA	N/A	infrared gas analyzer
k	m d^{-1}	gas transfer velocity
k_{600}	m d^{-1}	gas transfer velocity with a Schmidt number = 600
k_{CO2}	m d^{-1}	gas transfer velocity of carbon dioxide
k_{gas}	m d^{-1}	gas transfer velocity of a gas other than carbon dioxide
k_H	N/A	Henry's Law constant for solubility in water at stream temperature
pCO_2	μatm atm^{-1}	partial pressure of carbon dioxide

pH	mol L^{-1}	potential of hydrogen
Q	L s^{-1} or m^3 s^{-1}	discharge
RMSE	m d^{-1}	root mean square error
S	degrees or percentage	slope
Sc_{CO2}	N/A	Schmidt coefficient of carbon dioxide
Sc_{gas}	N/A	Schmidt coefficient of a gas other than carbon dioxide
T	ºC or K	temperature
t	s	time
V	m s^{-1}	velocity
ΔCO_2	µatm atm^{-1}	excess CO_2 in solution

Acknowledgements

I am incredibly grateful for the guidance and support I have received from mentors, colleagues, friends, and family throughout the process of completing this project. I thank my supervisor, Mark Johnson, and my supervisory committee member, Dan Moore, for their guidance, support, and patience in helping me develop as a researcher, regarding this project in particular but also through their respective courses. Additionally, this work was supported by an NSERC Discovery Grant to Mark Johnson.

I am very grateful for Iain Hawthorne's invaluable technical and field assistance and for the entire Ecohydrology Lab's support. I also thank Teddy Eyster, Kristi Collins, Michael Oh, Robin Arnold, Emma Luker, and Alida O'Connor for their field assistance. Further, I thank Zoran Nesic and Hughie Jones for their technical assistance, Brenda D'Acunha for her lab assistance, Ionut Aron for providing support at Malcolm Knapp Research Forest (and for saving me from getting stuck in the field twice), and Sally MacIntyre and Ted Tedford for their insightful conversations and imparting their expertise. Finally, I thank Rhy McMillan, whose editorial assistance and endless support have been a gift, the Miller-Vedam family, who have extended their home and love to me and therefore have supported me finishing this project immensely, and my family, who continues to support me from all over the continent, as they always have.

This research was conducted at the University of British Columbia, which is on the unceded traditional territory of the Musqueam First Nation. The field experiment was conducted at the Malcolm Knapp Research Forest, which is on the unceded traditional territory of the Katzie First Nation.

Dedication

For my sisters.

1 INTRODUCTION

Thorough characterization of the global carbon (C) cycle relies on accurate quantification of carbon fluxes into and out of all ecosystems. Among these fluxes, carbon dioxide (CO_2) evasion from surface waters has received increasing attention due to the active roles that streams, rivers, lakes, and estuaries play in transforming terrestrially-derived carbon (Aufdenkampe et al., 2011; Battin et al., 2009). In this way, inland waters significantly reduce the amount of terrestrial C that rivers ultimately deliver to the ocean (Cole et al., 2007).

Terrestrially-derived imports of C to a freshwater ecosystem are subsequently partitioned into C lost to the atmosphere through evasion, C stored in sediments, and C exported from the ecosystem through drainage (Cole et al., 2007). The majority of C inputs to streams and rivers are highly spatiotemporally variable (Wallin et al., 2011); they originate in the terrestrial environment, are transmitted via soils, and enter surface water systems through a range of hydrological flowpaths including groundwater-derived baseflow, shallow subsurface stormflow, and surficial runoff (Aufdenkampe et al., 2011). Headwater streams are particularly active sites of C cycling, not only because of their strong interactions with benthic substrates and the atmosphere (Benstead and Leigh, 2012), but also because they receive the majority of landscape drainage and are therefore closely coupled to terrestrial biogeochemical processes (Gomi et al., 2002).

A recent global estimate of 2.58 Pg C y^{-1} (Sawakuchi et al., 2017) suggests that almost half of terrestrially-derived C that enters streams and rivers is lost to the atmosphere through gaseous evasion, 36-64% of which evades from headwater streams (Marx et al., 2017; Raymond et al., 2013; Sawakuchi et al., 2017). Globally, pCO_2 values in headwater streams and effluxes of CO_2 from headwater streams are large but poorly constrained, resulting in

significant uncertainties in quantifying global C budgets (Butman and Raymond, 2011; Raymond et al., 2013; Marx et al., 2017).

Due to the considerably higher partial pressures of CO_2 (pCO_2) in headwater streams relative to pCO_2 in rivers (Butman and Raymond, 2011) and their proximity to terrestrially-derived C sources (Jones and Mulholland, 1998), many studies suggest that headwater streams are locations of substantial CO_2 evasion (Schelker et al., 2016; Wallin et al., 2013). However, current methodological limitations compromise our ability to thoroughly evaluate the significance of CO_2 fluxes between headwater streams and the atmosphere (Marx et al., 2017; Raymond et al., 2013). In particular, determination of the gas transfer velocity (k), a parameter that describes the rate of gas exchange across an air-water interface, presents a number of methodological challenges in headwater stream settings as it is spatiotemporally variable and dependent upon complex hydrogeomorphic stream properties (Raymond et al., 2012; Wallin et al., 2011).

In this study, I present an automated and field-deployable method for determining gas transfer velocities of CO_2 (k_{CO2}) in headwater streams. Accurate CO_2 evasion flux estimates from streams rely on frequent and accurate determinations of k_{CO2} that can be scaled with hydrogeomorphic and flow parameters for a given reach; difficulties in determining and scaling k_{CO2} therefore result in large uncertainties in calculating evasion fluxes. I also present relationships between k_{CO2} values of a headwater stream reach determined using this method and stream parameters measured including discharge, velocity, and temperature, as well as estimates of continuous CO_2 evasion from the reach. Thus, this method will allow researchers to determine k_{CO2} frequently and accurately in tandem with streamflow parameters, create site-specific scaling relationships, and calculate continuous CO_2 evasion fluxes from a reach.

The flux of CO_2 across an air-water interface (F_{CO2}, in g C L^{-1} d^{-1}) can be described in terms of the partial pressure gradient of CO_2 between air ($pCO_{2\ air}$, in μatm atm^{-1}) and water ($pCO_{2\ aq}$, in μatm atm^{-1}) and k_{CO2} (in m d^{-1}), such that:

$$F_{CO2} = k_{CO2} \times (pCO_{2\ aq} - pCO_{2\ air}) \quad (1)$$

Reorganizing equation (1), k_{CO2} can be calculated from F_{CO2}, $pCO_{2\ aq}$, and $pCO_{2\ air}$, such that:

$$k_{CO2} = (pCO_{2\ aq} - pCO_{2\ air}) / F_{CO2} \quad (2)$$

Specifically, k_{CO2} describes the height of a column of water that equilibrates with the atmosphere per unit of time (Frankignoulle et al., 1998; Wanninkhof et al., 2009).

In headwater streams, spatiotemporal variability in k_{CO2}, driven primarily by surface water turbulence, is the largest determinant of CO_2 effluxes (Hope et al., 2001; Tsivoglou and Neal, 1976; Zappa et al., 2007). Complex stream morphologies, including variable gradients and widths, streambed roughness, and tortuous flowpaths enhance the generation of surface water turbulence (MacIntyre et al., 1995; Wallin et al., 2011), with turbulence generally increasing with stream discharge and flow velocities (Billett and Harvey, 2013). Thus, the development of relationships between k_{CO2} and hydrogeomorphic and hydraulic parameters in headwater streams, calculated via accurate determinations of F_{CO2}, may allow for more accurate prediction of k_{CO2} and its scaling among different catchments and stream orders (Raymond et al., 2012).

Multiple methods exist for both experimentally determining and modeling k_{CO2}. Floating chambers can contain or be coupled to non-dispersive infrared (NDIR) sensors that directly and continuously monitor CO_2 in the chamber headspace and provide time-weighted mean values based on water-air headspace equilibration, from which the rate of CO_2 accumulation is measured (Alin et al., 2011; Campeau et al., 2014; Vachon et al., 2010).

However, researchers criticize this method due to inherent chamber effects on surface water turbulence and modified conditions inside the chamber (Gafalk et al., 2013; Crawford et al., 2014; Raymond and Cole, 2001). Additionally, some studies use the eddy covariance technique to determine k_{CO2} and F_{CO2} in large rivers (Huotari et al., 2013) and lakes (Jonsson et al., 2008), which allows for accurate and direct measurement of CO_2 fluxes at the ecosystem scale (Huotari et al., 2013). However, this method is not appropriate for small streams, because it requires a large fetch area around the measurement location (Wallin et al., 2011).

Due to the limitations for floating chamber use, particularly for highly turbulent streams, tracer gas injections have become the most widely-used and robust method for determining k_{CO2} in headwater streams (Natchimuthu et al., 2017; Öquist et al., 2009; Tobias et al., 2009). This method involves injecting an inert volatile gas tracer (e.g., sulfur hexafluoride (SF_6), propane (C_3H_8), or methyl chloride (CH_3Cl)) and measuring its loss over a specified stream reach (MacIntyre et al., 1995; Wanninkhof et al., 1990). After adequate mixing has occurred, sampling of the stream in two locations downstream of the gas injection site allows for determination of the tracer concentration via headspace analysis on a gas chromatograph. The resulting k_{tracer} is then converted to k_{CO2} using Schmidt dependences (e.g., Clark et al., 1995; Kokic et al., 2015; Looman et al., 2016). The conversion requires empirically-derived coefficients for both gases, as expressed in the following equation:

$$k_{tracer} / k_{CO2} = (Sc_{tracer} / Sc_{CO2})^{-n} \quad (3)$$

where Sc is the Schmidt number, defined as the ratio of the kinematic viscosity of water and the diffusion coefficient of the gas (Raymond et al., 2012), and n is the Schmidt number exponent, which is assigned a value of 1/2 to 2/3 depending on the surface state of the water (Jähne et al., 1987). Frequently, researchers couple tracer gas injection with a non-volatile

solute tracer injection (e.g., NaCl) to determine discharge and the travel time of the reach length (Genereux and Hemond, 1992; Marzolf et al., 1994; Shaw et al., 2010).

Tracer gas injections have been the preferred method for experimentally determining k_{CO2} in headwater streams as they do not affect the air-water interface, while providing an integrated measure of the exchangeability of CO_2 in a stream reach at a specific point in time (Marx et al., 2017; Wallin et al., 2011). However, due to the manual nature of gas injection, stream sampling, and laboratory analysis, most tracer gas experiments do not readily allow for frequent sampling or continuous monitoring (Marx et al., 2017).

In a metadata analysis of 563 tracer gas experiments, Raymond et al. (2012) determined relationships between *k* and stream hydraulic and slope parameters and reported seven regression equations (mean $r^2 = 0.63$). Although these equations perform well over large spatial scales, the authors cautioned that direct measurements of *k* are still necessary in small-scale studies. In particular, systems with high slopes and velocities, such as headwater catchments, require direct measurements to accurately determine *k* (Raymond et al., 2012; Wallin et al., 2011). Additionally, measurements of *k* made at high spatial and temporal frequencies, especially those that capture diurnal, seasonal, hydrologic, and climatic variability, will aid in accurately determining flux measurements (Marx et al., 2017).

To address these issues, I developed an automated method to determine k_{CO2} using CO_2 as a tracer. I tested this approach under a range of flow conditions for a first-order stream of a headwater catchment in southwestern British Columbia, Canada. I used two *in situ* infrared gas analyzing (IRGA) CO_2-type sensors enclosed in waterproof, gas-permeable membranes (Johnson et al., 2010) to continuously measure pCO_2 downstream from a CO_2 gas diffuser that delivered periodic injections of CO_2 to the stream environment. Using CO_2 as a tracer presents

advantages of being automatable and field-deployable, and it does not require supplemental gas chromatography or conversions via Schmidt dependences, as is the case for most tracer gas experiments. Thus, it can be used to make measurements at different temporal resolutions, including at night, or in response to events of scientific interest, such as storms. The automation and programmability of this method will allow researchers not only to augment current datasets of k_{CO2}, but also to readily scale k_{CO2} with hydrogeomorphic parameters.

In the present study, I deployed this autonomous system to enable frequent and accurate determinations of k_{CO2} across a range of flow conditions. I hypothesized that a high stream slope and turbulent sections within the reach would result in high k_{CO2} values overall, and that k_{CO2} would correspond positively with flow parameters (e.g., discharge and stream velocity). Multiple determinations of k_{CO2} obtained during varying flow conditions allowed me to interpolate k_{CO2} values for the entire study period and calculate continuous CO_2 emissions from the stream. As headwater systems are known to be "hotspots" for CO_2 evasion, the proof of concept presented here suggests a route forward for better elucidating the role that CO_2 fluxes from headwater streams play in the global C cycle.

2 METHODS

2.1 Site description

I conducted the research reported on in this thesis at the University of British Columbia Malcolm Knapp Research Forest (MKRF) located in Maple Ridge, British Columbia, approximately 60 km east of Vancouver (49°16'N 122°34'W) (Figure 1). MKRF is located in the Fraser Valley of British Columbia and the Coastal Western Hemlock Biogeoclimatic Zone. It typically experiences mild, wet winters and warm, dry summers. At upper East Creek in

MKRF, mean annual precipitation is 2353 mm yr^{-1}, mean annual temperature is 9°C, and mean monthly temperature ranges from 1.4-16.8°C (Richardson and Moore, 2010).

MKRF primarily contains a mixture of Douglas fir, western hemlock, and western red cedar, as well as big leaf maple, black cottonwood, and red alder (Turk et al., 1998). The understory vegetation primarily consists of vine maple, western sword fern, salal, and trailing blackberry (Turk et al., 1998). The soil is a Gleyed Brunisol with dominant textures of sandy loam and loamy sand (Tashe 1998). Parent material consists primarily of colluvium and till (Klinka 1976).

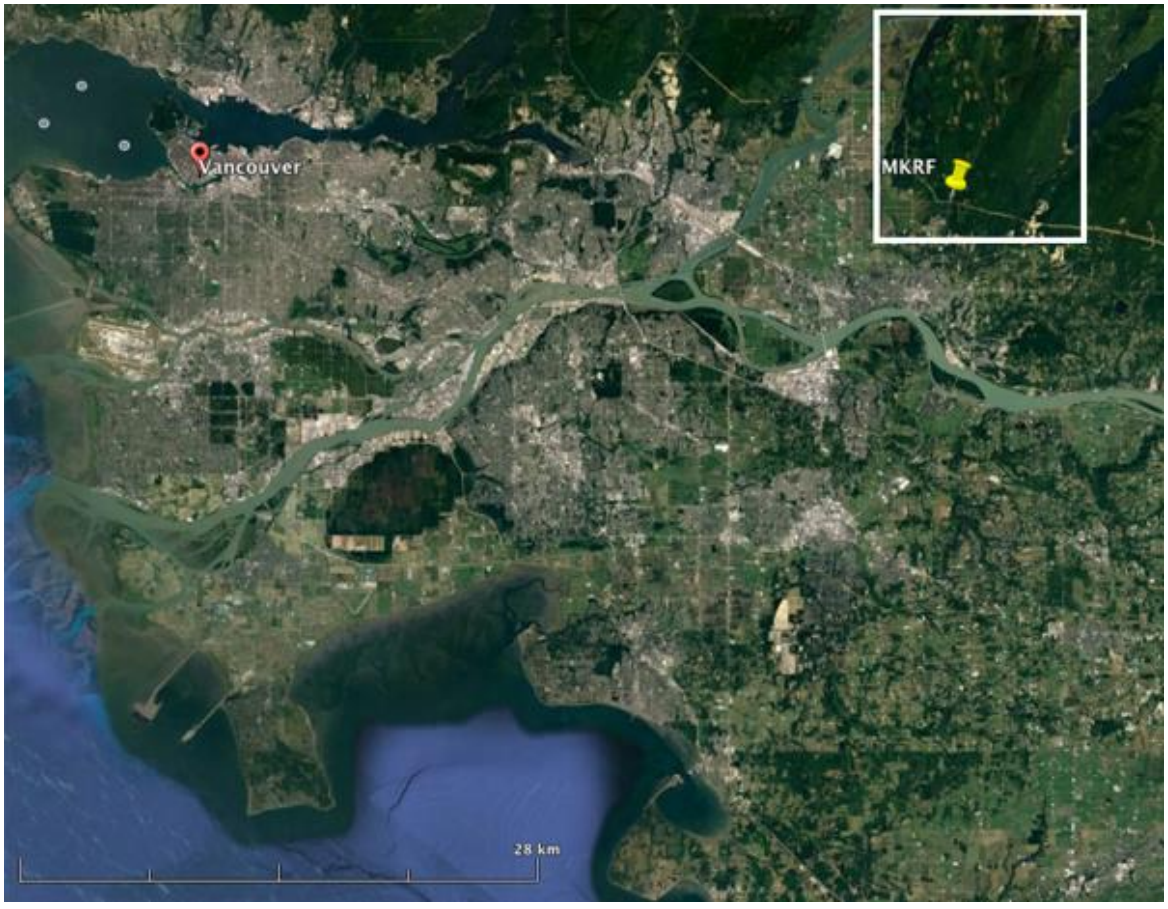

Figure 1. Location of the UBC Malcolm Knapp Research Forest within southwestern British Columbia, Canada. (Google Earth)

This work was carried out in experimental stream “G-H”, located in the southeastern part of MKRF (Figure 2). The 64-m reach of G-H used in the present study flows southwest below a debris jam and a weir at the outlet. The mean width of the reach is 4 m and the mean slope is 0.236 (13.3°). The reach is heavily shaded by vegetation, with a steep southeastern riparian area and a shallower northwestern riparian area intersected by a logging road. Riffle-run sequences dominate the upper part of the reach, generating turbulence, with variable depth pools more common in the lower part of the reach. Many streams in MKRF, G-H included, partially or entirely dry up in the summer months. The catchment for G-H is 0.54 km^2 and ranges in elevation from 235–330 m.

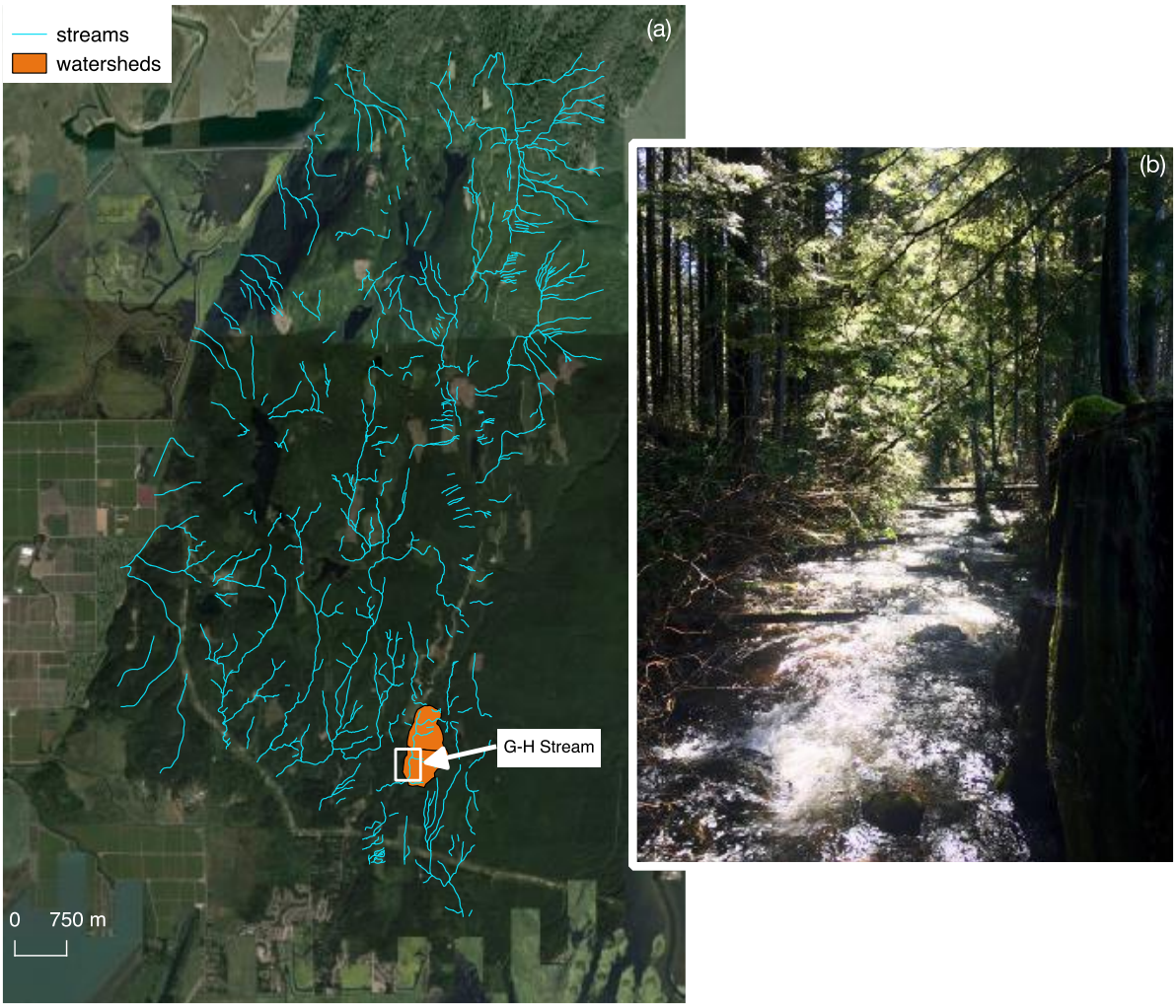

Figure 2. (a) Location of study reach in experimental stream G-H (white box) within MKRF (designated by roads and streams), and (b) study reach in experimental stream G-H. Photo taken on March 18, 2017; perspective is facing downstream. (Google Earth)

2.2 Experimental setup

A weir hut located on the stream bank at the outlet of the reach provided protection for a power supply and data acquisition system. A 12-V battery supplied power to a Campbell Scientific CR1000 datalogger and AM16/32B multiplexer, two IRGA CO_2-type gas

analyzing sensors, six water quality sensors, a sonic anemometer, a wireless modem, and a solenoid valve connected to a compressed gas cylinder (Table 1).

Table 1. Descriptions, manufacturers, measured parameter(s) (for this experiment), and accuracy of sensors used in experiment.

Sensor	**Manufacturer**	**Parameter(s) measured**	**Accuracy**
GMP221	Vaisala	pCO_2	±1% of range + 2% of reading
CSIM11-L	Campbell Scientific	pH	±0.1% over full range
GS3	Decagon	electrical conductivity stream temperature	±10% (EC) ±1 ºC (stream temperature)
CTD-10	Decagon	depth	0.05% of full scale at 20 ºC
81000 ultrasonic anemometer	RM Young	air temperature wind speed wind direction	±2 ºC (air temperature) ±0.05 m s^{-1} (wind speed) ±2º (wind direction)

Sensors were distributed between two groups, each of which was fixed on the stream bed: one group at the reach halfway point (32 m from diffuser) and one at the end of the reach (63 m from diffuser). Each group contained the following sensors: a Vaisala GMM220 transmitter module with a GMP221 CO_2 probe (Vantaa, Finland), a Campbell Scientific CSIM11-L pH probe (Logan, Utah, USA), a Decagon GS3 ruggedized soil moisture, temperature, and electrical conductivity probe (Pullman, Washington, USA), and a Decagon CTD-10 electrical conductivity, temperature, and depth probe. Figure 3 provides a schematic diagram of field setup. The stream parameter values discussed below reflect measurements from the upstream

group of sensors, which were located mid-reach and were shaded by forest cover. The downstream portion of the reach was less fully shaded due to proximity to the weir and weir hut. An RM Young Model 81000 ultrasonic anemometer (Traverse City, Michigan, USA) was situated 2 m above the ground on the stream bank between the upstream and downstream sensors.

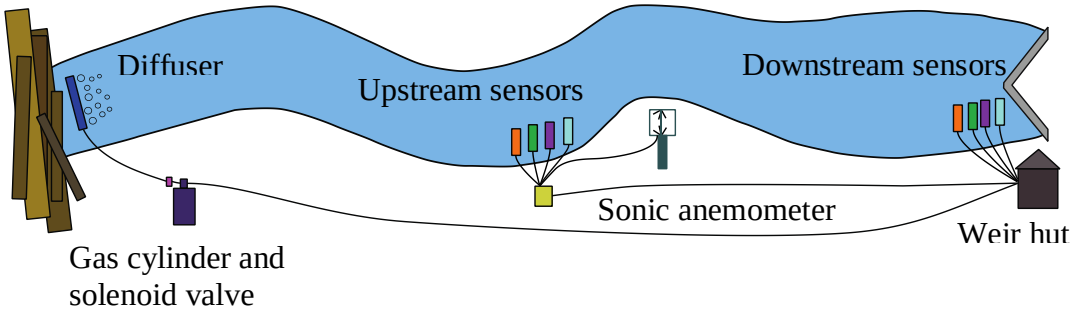

Figure 3. Schematic diagram of field setup. *In situ* stream sensors include IRGA CO_2 probes, pH probes, CTD, and GS3 (upstream and downstream sensor bundles are identical). The weir hut contains the CR1000 datalogger and battery.

The datalogger program provided commands for the sensors and solenoid valve through the datalogger and multiplexer, and it compiled sensor outputs into two data tables (see Appendices 1 and 2 for CR1000 programs). The main program collected continuous data from most sensors at a 5-second scan interval, averaging data into 30-minute averages. The IRGA sensors, with 4W demand each, were programmed to turn on for the last five minutes of each half-hour time block. This 30-minute data table collected data continuously and generated 48 distinct values for each measured component per day. During gas injection

periods, described in detail below, which occurred twice daily for an hour per injection (5-6 am and 5-6 pm local time), the datalogger collected data from all sensors at 5-second intervals, storing this higher frequency data in a separate table. A cellular modem was turned on daily between 8-9 am local time, and the datalogger transmitted both data tables to a UBC laboratory computer.

A data gap from December 25, 2016, to January 22, 2017, resulted from a period when access roads at the site were impassable due to snow and power to the system was lost due to an interruption in battery swaps. Other data gaps reflect tracer addition periods (CO_2 injections or salt additions used for discharge determination), as well as periods removed due to sensor issues.

2.3 CO_2 injection and gas transfer velocity calculation

During gas injection periods, a solenoid valve was used to switch the CO_2 injection gas flow on for one hour, allowing the compressed gas cylinder to continuously deliver industrial-grade CO_2 at a streamflow-dependent flow rate of 5 L min^{-1} – 10 L min^{-1}. CO_2 flowed from the cylinder via U.S. Plastic Corporation Bev-A-Line tubing (Lima, Ohio) to a 1-meter long aquatic diffuser situated on the stream bed at the inlet of the reach, just below the debris dam. Upstream and downstream IRGAs recorded increasing pCO_2 values as the injected CO_2 dissolved and mixed into the reach, eventually equilibrating at elevated concentrations during the injection. The relative differences between baseline and elevated values for each sensor were used in calculation of k_{CO2}.

Henry's Law was used to determine the mass equivalence of dissolved CO_2 (here expressed as in carbon equivalent terms as mg CO_2-C L^{-1}) as a function of stream temperature

and pCO_2 in solution (Plummer and Busenberg, 1982). The difference between upstream and downstream mass equivalences of CO_2-C allowed me to calculate the evasion flux of CO_2 along the stream reach. This information, in combination with excess CO_2 in solution, permitted determination of k_{CO2} using the variables listed in Table 2 via the equations given in Table 3. For the purpose of compatibility with existing literature, I report both k_{CO2} and k normalized to a Schmidt number of 600 (k_{600}), which corresponds to a temperature of 20ºC for CO_2 (Jähne et al., 1987). k_{CO2} can be converted to k_{600} using the following equation:

$$k_{600} = k_{CO2} \text{ x } (600 / Sc_{CO2})^{-0.5} \quad (4)$$

I calculated k_{CO2} and k_{600} from 49 CO_2 injections, discarded 6 negative and 5 very large outliers, and used the remaining 38 discrete measurements of k_{CO2} and k_{600} for assessing relationships with other variables. Negative k_{CO2} and k_{600} values are not physically meaningful in this stream due to continual CO_2 supersaturation in streamwater and high turbulence. Issues regarding the gas cylinder setup and harsh winter weather presented challenges through February 2017, so the k_{CO2} and k_{600} values reported here were determined during the last four months of the experiment.

Table 2. Variables used in calculation of k_{CO2}.

Symbol	Description (units) [constant]
k_H	Henry's Law constant for solubility in water at stream temperature
T	Temperature (K)
$k_H^{\ominus}$	Henry's Law constant for solubility in water at standard temperature and pressure (STP) [0.035]
D	Temperature dependence constant (K) [2400]
$T^{\ominus}$	Temperature at STP (K) [298.15]
C	Mass equivalence of dissolved CO_2 (mg CO_2-C L^{-1})
CO_2	pCO_2 resulting from injection relative to baseline (atm)
ΔCO_2	Excess CO_2 in solution (atm)
$CO_{2(aq)}$	Mean pCO_2 in stream (atm)
$CO_{2(air)}$	pCO_2 in atmosphere (atm)
F	CO_2 evasion flux along reach (g C L^{-1} d^{-1})
d	Depth (m)
t	Travel time between salt slug centroids (s)
k_{CO2}	Gas transfer velocity (m d^{-1})

Table 3. Equations used in calculation of k_{CO2}.

Equation
$k_{\mathrm{H}(1)} = k_{\mathrm{H}}^{\ominus} \times \exp\left(D\left(\frac{1}{T_{(1)}} - \frac{1}{T^{\ominus}}\right)\right)$
$k_{\mathrm{H}(2)} = k_{\mathrm{H}}^{\ominus} \times \exp\left(D\left(\frac{1}{T_{(2)}} - \frac{1}{T^{\ominus}}\right)\right)$
$k_{\mathrm{H}(mean)} = k_{\mathrm{H}}^{\ominus} \times \exp\left(D\left(\frac{1}{T_{(mean)}} - \frac{1}{T^{\ominus}}\right)\right)$
$C_{(1)} = k_{\mathrm{H}(1)} \times \mathrm{CO}_{2(1)} \times 12$
$C_{(2)} = k_{\mathrm{H}(2)} \times \mathrm{CO}_{2(2)} \times 12$
$\Delta\mathrm{CO}_2 = k_{\mathrm{H}(mean)} \times \left(\mathrm{CO}_{2(aq)} - \mathrm{CO}_{2(air)}\right) \times 12$
$F = \frac{C_{(1)} - C_{(2)}}{t}$
$k_{\mathrm{CO2}} = \frac{\Delta CO_2 \times d}{F}$

2.4 Field measurements, sensor calibration, and sensor maintenance

Many *in situ* sensors require both pre-deployment and routine calibration and maintenance to ensure proper functioning and data validity. Before sensor installation, I wrapped all sensors except the two CTDs in a protective perforated PVC wrap. Sensors were individually calibrated according to manufacturer calibration instructions. While the CTD sensors provide information on stream water EC, the EC output from the GS3 sensors has

higher resolution, enabling the development of stage-discharge relationships described below. I performed sensor maintenance on weekly field visits, except when logging roads in MKRF were impassable due to snow (much of January and February 2017). During field visits and where applicable, I cleaned all sensors with water or soapy water and a cloth, flushing any sediment or debris that accumulated in the protective PVC wrap. I used a Hanna Low Range pH/Conductivity/TDS PPM Tester HI98129 (Woonsocket, Rhode Island, USA) to obtain weekly pH values against which the continuously recorded pH values could be adjusted based on standard methods for *in situ* water quality sensors (Gibs et al., 2007).

Prior to installation, I calibrated the IRGA sensors using the Vaisala CARBOCAP Carbon Dioxide Calibrator (GMK220) according to the two-point calibration procedure described in the manual (Vaisala Oyj, 2006). During field visits, I checked the calibration of the IRGA sensors by deploying a third IRGA sensor next to the *in situ* sensors for a few minutes and ensured that the outputs were similar. This check ensured that both deployed sensors continued to perform in a similar manner and without drift throughout the study. Deployment of a third IRGA also allowed me to survey the stream reach for areas of potential groundwater inputs which could locally elevate pCO_2, as well as to assess changes in pCO_2 along the reach during several gas injections.

The functionality of an IRGA sensor in an aqueous environment requires that the light-source, detector, and gas bench are enclosed within a waterproof, gas-permeable membrane (Johnson et al., 2010). Both IRGA sensors were encased in polytetrafluoroethylene (PTFE) sleeves and sealed with liquid electrical tape according to the method described in Johnson et al. (2010). Diffusivity measurements of the sleeve indicate that it has a negligible effect on CO_2 diffusion and sensor response time (Johnson et al., 2010).

I measured stream discharge using salt additions as described in Moore (2005) and Richardson et al. (2017) to develop a rating curve for the stream, as the V-notch on the weir was greater than 90º. Using this method, I added 100 g of salt (NaCl) dissolved in 1 L streamwater to the top of the reach and recorded EC with the upstream and downstream GS3 sensors as the salt addition passed. I calculated discharge by integrating the downstream salt pulse, using a calibration constant of 0.486 $mg \cdot NaCl \cdot cm \cdot \mu S^{-1} \cdot L^{-1}$ (Richardson et al., 2017), taking the mean values based on two repeated salt additions. The travel time between centroid of the salt pulse as it passed each EC sensor was used to determine modal stream velocity (V) (Waldon 2004). I subsequently evaluated relationships between stage, discharge, and velocity using regression models. These relationships were used to calculate continuous discharge and velocity for the entire dataset, as well as to determine the CO_2 evasion dynamics and gas travel time between IRGA sensors during CO_2 injections.

2.5 Gas transfer velocity data analysis and method validation

Data analysis was conducted in R version 3.3.3 (R Core Team, 2017). I determined logarithmic linear regression relationships between k_{CO2} and k_{600} and hydraulic stream properties, including stream discharge, velocity, and temperature. I compared the k_{600} values determined using this method to outputs from seven models of k_{CO2} (Table 4) based on hydrogeomorphic variables described in Raymond et al. (2012). Continuous long-term data are presented as 6-hourly averages to reduce overplotting.

Table 4. Seven models for predicting k_{600} (m d^{-1}) based flow velocity (V, in m s^{-1}), slope (S, unitless), stream depth (D, in m), discharge (Q, in m^3 s^{-1}), and the Froude number ($Fr = V/(gD)^{0.5}$), described in Raymond et al. (2012).

Model equation
$k_{600} = (VS)^{0.89 \pm 0.020} \times D^{0.54 \pm 0.030} \times 5037 \pm 604$
$k_{600} = 5937 \pm 606 \times (1 - 2.54 \pm 0.223 \times Fr^2) \times (VS)^{0.89 \pm 0.017} \times D^{0.58 \pm 0.027}$
$k_{600} = 1162 \pm 192 \times S^{0.77 \pm 0.028} \times V^{0.85 \pm 0.045}$
$k_{600} = (VS)^{0.76 \pm 0.027} \times 951.5 \pm 144$
$k_{600} = VS \times 2841 \pm 107 + 2.02 \pm 0.209$
$k_{600} = 929 \pm 141 \times (VS)^{0.75 \pm 0.027} \times Q^{0.011 \pm 0.016}$
$k_{600} = 4725 \pm 445 \times (VS)^{0.86 \pm 0.016} \times Q^{-0.14 \pm 0.012} \times D^{0.66 \pm 0.029}$

2.6 Continuous CO_2 emissions estimates

I determined continuous k_{CO2} and k_{600} for the entire study period using the linear regression relationships between log(k_{CO2}), log(k_{600}), and discharge. Back-transforming logarithmic regression models requires a bias correction and uncertainty calculation (Baskerville, 1972). A regression model of the form:

$$\log(y) = x = b_0 + b_1 x + e \quad (5)$$

can be solved using the original terms and the sample residual variance of the logarithmic equation (σ), in which (Baskerville, 1972):

$$y = e^{(x + \sigma/2)} \quad (6)$$

The estimated variance in y (σ_A) can be calculated via (Baskerville, 1972):

$$\sigma_A = e^{(2\sigma + 2x)} - e^{(\sigma + 2x)} \quad (7)$$

I determined continuous CO_2 emissions from the stream using Equation (2), with continuous k_{CO2}, continuous dissolved pCO_2, and the average atmospheric pCO_2 above the reach (427 μatm atm^{-1}), with the latter determined via headspace analysis on a gas chromatograph (Kling et al., 1991) (See Appendix 3 for description of analysis). I also determined regression relationships between continuous CO_2 emissions and continuous stream discharge and velocity.

3 RESULTS

3.1 Continuous monitoring of stream and environmental parameters

3.1.1 Weather

Precipitation at MKRF totaled 1387 mm over the study period (November 2016 – June 2017). Mean air temperature during the study period was 4 ºC and ranged from -11 to +21 ºC (Figure 4). Mean wind velocity measured within the forest and adjacent to the stream was 0.3 m s^{-1} and ranged from 0.004 – 0.94 m s^{-1}, with about half of all observations originating from the north and northeast (Figure 5). Table 5 provides monthly rainfall totals and average temperatures for the study period as well as 30-year means.

3.1.2 CO_2 variability and stream chemistry

Baseline pCO_2 values ranged from 1133 – 2110 μatm atm^{-1} over the study period, with mean and median values of 1434 and 1404 μatm atm^{-1} (Figure 4). Streamwater pCO_2 decreased slightly between November and February, and diurnal variation remained relatively stable and limited between November and April. Both pCO_2 and diurnal variation increased during May

and June. See Table 6 for mean and median values and ranges of pCO_2 during each month of the study period. Streamwater pH ranged from 6.5 – 7.2, with an average value of 6.9.

Stream temperature ranged from 0.3 – 15.2 ºC during the study period, with a mean value of 7 ºC (Figure 4). Electrical conductivity remained relatively low, with mean and median values of 12 and 11 μs cm^{-1} and a range of 10 – 19 μs cm^{-1} (Figure 4).

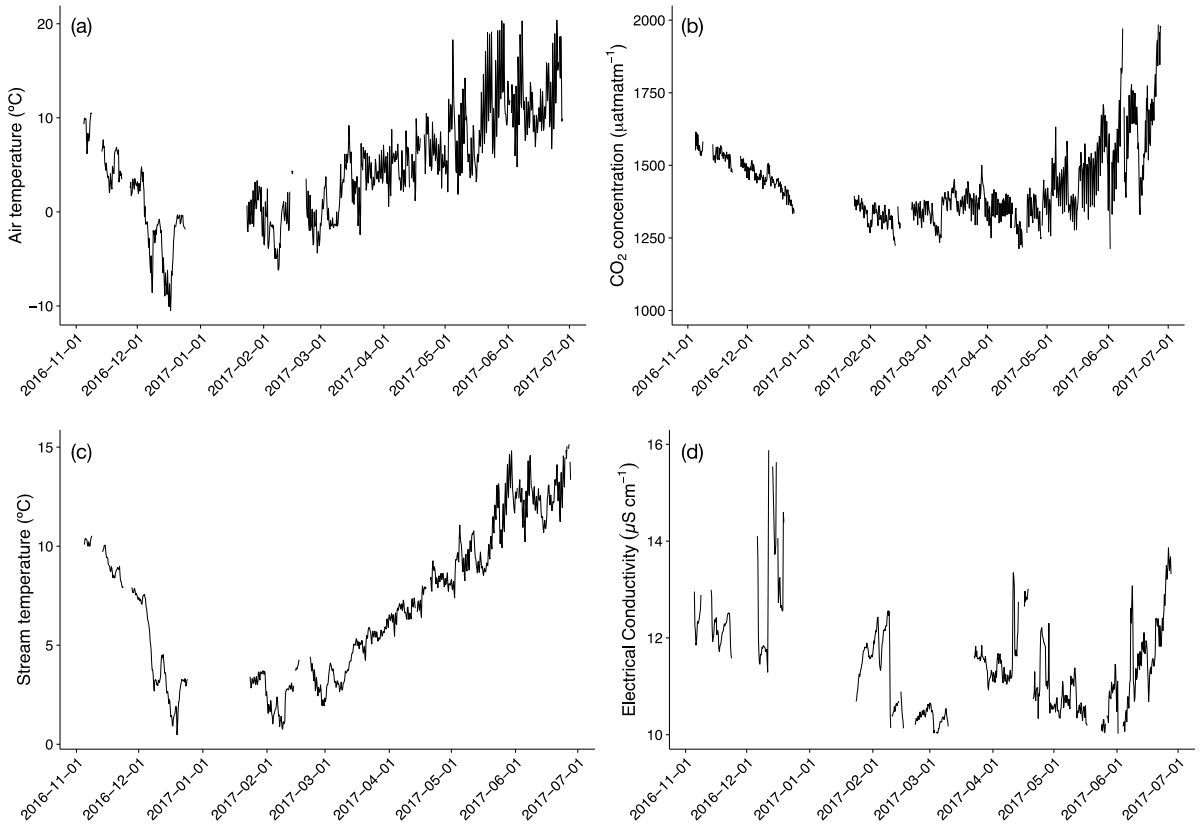

Figure 4. Time series of 6-hour time-averaged (a) air temperature, (b) pCO_2, (c) stream temperature, and (d) electrical conductivity observations during the study period.

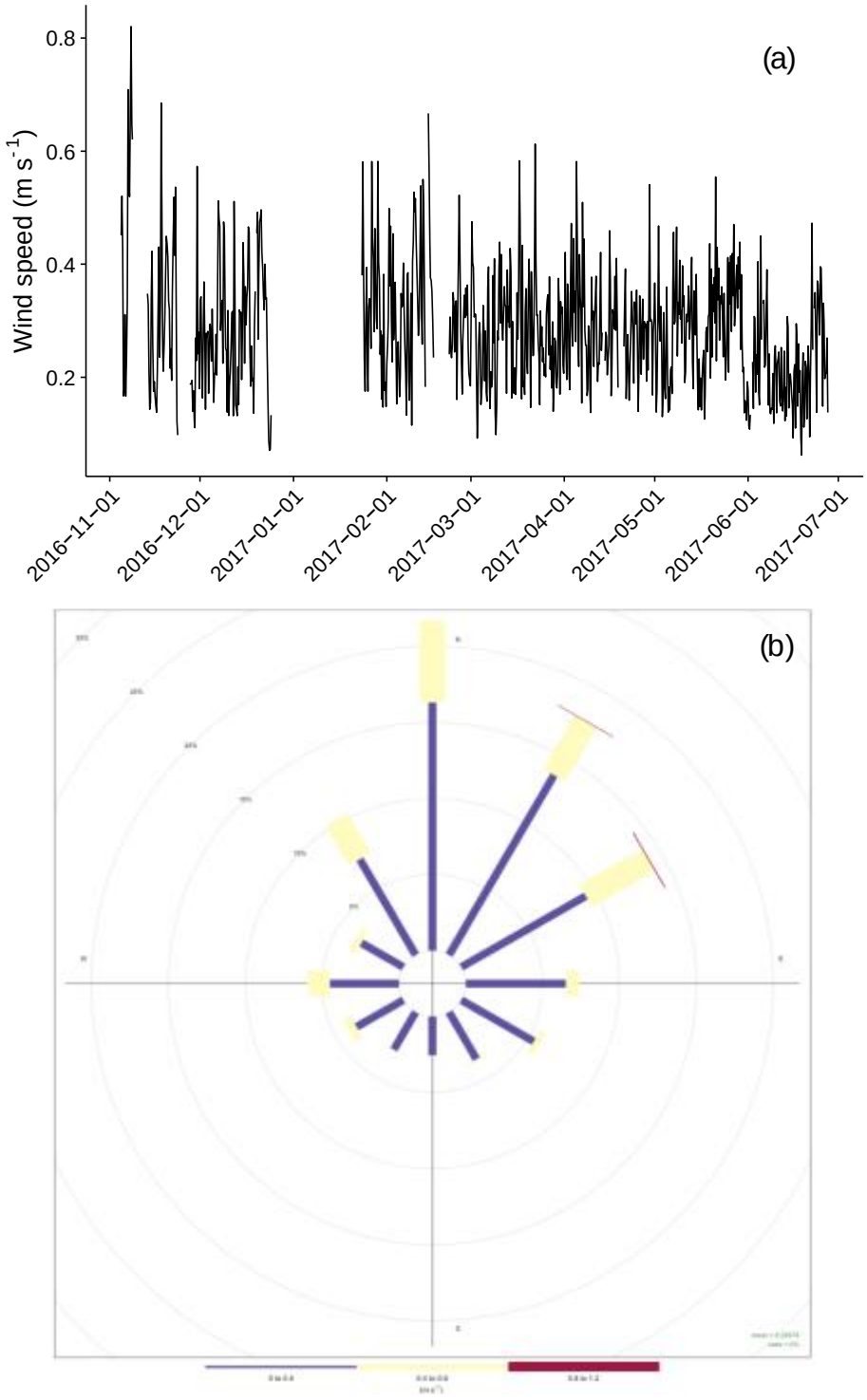

Figure 5. (a) Time series of 6-hour time-averaged wind speed observations during the study period and (b) wind rose of frequencies of 30-minute time-averaged wind speed observations by direction during the study period.

Table 5. Monthly rainfall totals (mm) and average (ºC) temperatures during the study period and 30-year means.

Month	Rainfall (mm)		Temperature (ºC)	
	Study period	30-year mean	Study period	30-year mean
November	310	334	5.3	5.3
December	254	289	-2.5	2.4
January	137	259	0.4	2.2
February	167	230	-1.6	4
March	326	209	2.7	6.2
April	176	161	5.5	9.1
May	131	136	9.3	12.4
June	21	107	11.5	15.1

Table 6. Mean and median stream pCO_2 values during each month of the study period.

Month	mean pCO_2 ($\mu atm\ atm^{-1}$)	median pCO_2 ($\mu atm\ atm^{-1}$)
November	1531	1533
December	1442	1444
January	1349	1355
February	1327	1330
March	1365	1372
April	1347	1350
May	1458	1449
June	1637	1623

3.2 Discharge determinations from salt slug injections

I calculated discharge, velocity, and travel time between salt pulse centroids based on data recorded by two electrical conductivity sensors from 24 salt additions between January and May, 2017. Of these calculations, 19 were used to model regression relationships between hydrologic variables and stage, while 5 were discarded as statistical outliers due to a poor relationship with discharge. Non-linear regression models that predicted stream discharge, stream velocity, and travel time using stage as an external regressor performed well, with r^2 values of 0.95 ($p < 0.001$), 0.90 ($p < 0.001$), and 0.86 ($p < 0.001$), respectively (Table 7). Calculated stream discharge during salt additions ranged from 56.8 L s^{-1} – 438 L s^{-1}, and calculated velocities during salt additions ranged from 0.11 – 0.46 m s^{-1}. Travel times for the 31 m between groups of sensors ranged from 70 s at higher flows to 295 s at lower flows.

Table 7. Equations, coefficients of determination, and p-values of regression models that predict discharge (Q), flow velocity (V), and slug travel time (T) from stage (D), based on calculations from salt slug injections (n = 19).

Equation	**r^2**	**p-value**
$Q = 0.005 \times D^{1.856}$	0.95	< 0.001
$V = 0.001 \times D - 0.036$	0.90	< 0.001
$T = 72944 \times D^{-1.105}$	0.86	< 0.001

3.2.1 Hydrology

The hydrograph over the study period (Figure 6) indicated rapid responses to frequent storm events, with discharge surpassing 400 L s^{-1} during six events throughout the study

period. Overall, discharge was higher during the rainy months of November and December and lower in late January and throughout February, which were uncharacteristically cold and snowy compared to the long-term record. Higher discharge resumed with spring rains in March. Mean and median discharge during the study period was 117.2 and 92.6 L s^{-1}, respectively, and ranged from 9.2 – 601.5 L s^{-1}. Mean flow velocity over the study period (Figure 6) ranged from 0.02 – 0.45 m s^{-1}, with mean and median values of 0.15 and 0.14 m s^{-1}, respectively.

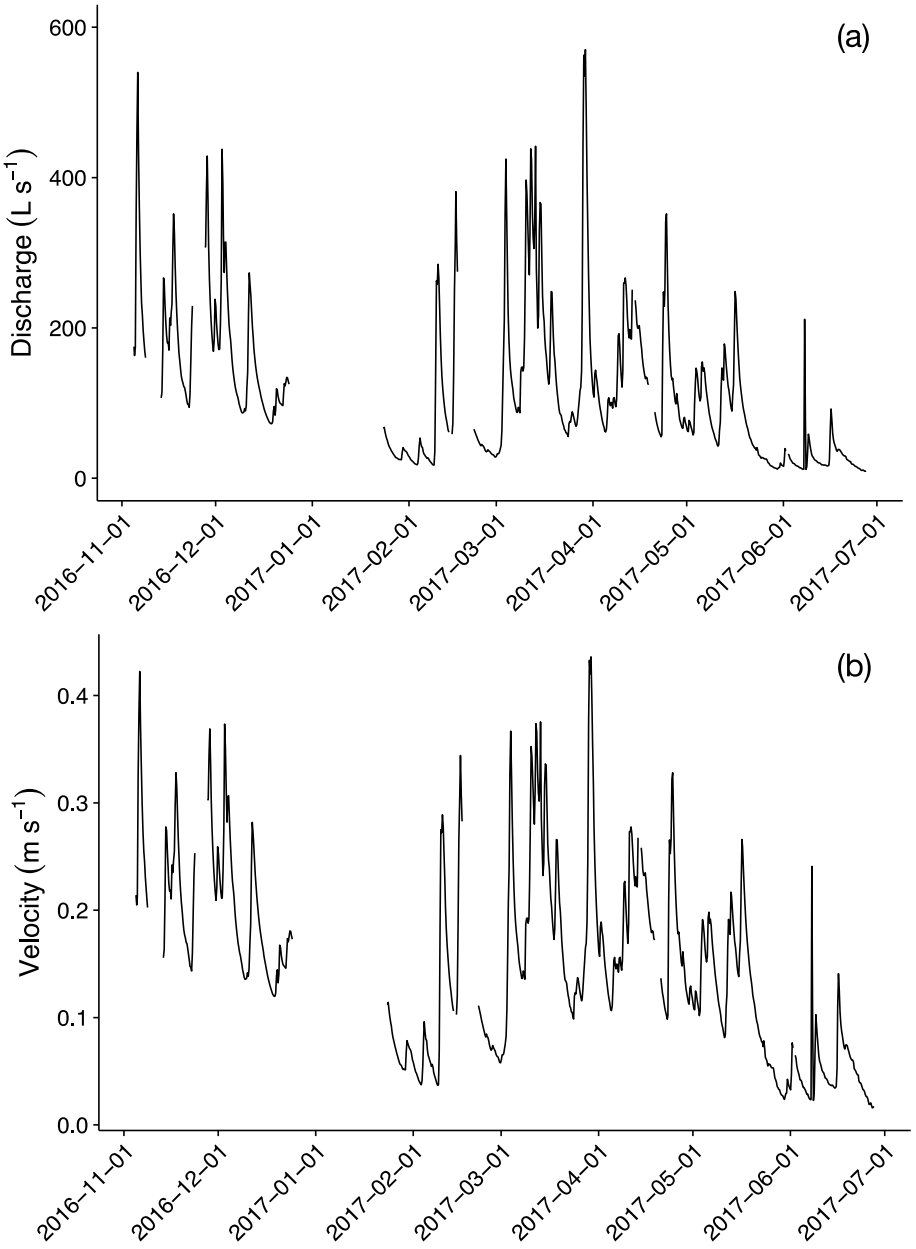

Figure 6. Time series of 6-hour time-averaged (a) stream discharge and (b) velocity during the study period.

3.3 Gas transfer velocity estimates

Mean and median k_{CO2} values were 48.9 and 31.4 m d^{-1}, respectively, and ranged from 18.32 to 186.16 m d^{-1}. Mean and median k_{600} values were 66.0 and 42.3 m d^{-1}, respectively,

and ranged from 20.4 to 261 m d^{-1}. Values for k_{CO2} and k_{600} as well as discharge, stream velocity, and stream temperature values during each CO_2 injection are given in Table 8.

Table 8. Values calculated from 38 CO_2 injections: gas transfer velocities (k_{CO2}), gas transfer velocities normalized to a Schmidt number of 600 (k_{600}), stream discharge (Q), stream velocity (V), and stream temperature (T).

k_{CO2} (m d^{-1})	k_{600} (m d^{-1})	Q (L s^{-1})	V (m s^{-1})	T (ºC)
82.46	118.34	264.97	0.28	6.51
116.60	162.36	230.53	0.25	7.65
105.26	148.76	194.54	0.23	7.09
82.44	115.65	199.32	0.23	7.37
77.33	108.80	182.23	0.22	7.26
186.16	260.98	266.37	0.28	7.39
136.99	194.78	247.48	0.27	6.86
74.22	103.92	220.25	0.25	7.44
55.85	79.10	201.42	0.23	7.01
65.07	88.89	100.73	0.15	8.37
29.26	40.14	66.64	0.11	8.22
32.33	44.38	80.05	0.13	8.20
47.07	64.24	70.52	0.12	8.42
22.17	29.01	50.51	0.09	10.02
21.23	27.26	44.53	0.08	10.73
55.61	73.41	122.56	0.17	9.68

35.25	45.09	115.31	0.16	10.90
26.55	34.31	101.32	0.15	10.50
72.04	93.73	153.64	0.20	10.24
53.31	71.52	141.49	0.19	9.07
55.60	73.55	137.98	0.18	9.60
38.27	52.04	114.32	0.16	8.55
34.04	44.78	98.16	0.15	9.82
26.41	35.68	84.74	0.13	8.81
25.37	33.28	73.12	0.12	9.93
26.95	36.07	64.95	0.11	9.16
22.84	29.75	57.19	0.10	10.20
27.31	33.87	20.47	0.04	12.08
29.08	35.08	19.36	0.04	13.17
30.44	37.55	18.67	0.04	12.30
26.25	30.94	16.86	0.04	14.08
27.30	32.73	15.69	0.03	13.41
19.16	21.85	13.80	0.03	15.39
19.03	21.97	12.96	0.03	14.91
18.83	20.96	11.16	0.02	16.39
18.38	20.81	10.65	0.02	15.71
18.32	20.43	9.94	0.02	16.30
18.92	22.20	9.59	0.02	14.26

3.3.1 Relationships between gas transfer velocities and stream parameters

Overall, I found that k_{CO2} and k_{600} were positively associated with stream discharge, with low values at low discharge (Q < 100 L s^{-1}) and high values at high discharge (Q > 100 L s^{-1}) (Figure 7). Mean values of k_{CO2} and k_{600} at low discharge were 25.8 and 32.5 m d^{-1}, and mean values of k_{CO2} and k_{600} at high discharge were 77.6 and 107 m d^{-1}. Similarly, k_{CO2} and k_{600} were positively associated with stream velocity, with low values at low velocity (V < 0.13 m s^{-1}) and high values at high velocity (V > 0.13 m s^{-1}) (Figure 8). Mean values of k_{CO2} and k_{600} at low flow velocity were 25.3 and 31.7 m d^{-1}, and mean values of k_{CO2} and k_{600} at high velocity were 72.6 and 100 m d^{-1}. k_{CO2} and k_{600} were inversely related to stream temperature, with low values at high temperature (T > 10 ºC) and high values at low temperature (T < 10 ºC) (Figure 9). Mean values of k_{CO2} and k_{600} at low stream temperature were 67.0 and 92.9 m d^{-1}, and mean values of k_{CO2} and k_{600} at high stream temperature were 26.7 and 32.8 m d^{-1}

Of the 38 CO_2 injections, 21 were conducted during the day, and 17 were conducted at night. Mean values of k_{CO2} and k_{600} during daytime and nighttime were 51.4 and 69.0 m d^{-1} and 45.9 and 62.3 m d^{-1}, respectively. Although daytime values were slightly higher, interquartile ranges of daytime and nighttime k_{CO2} and k_{600} overlapped significantly (Figure 10).

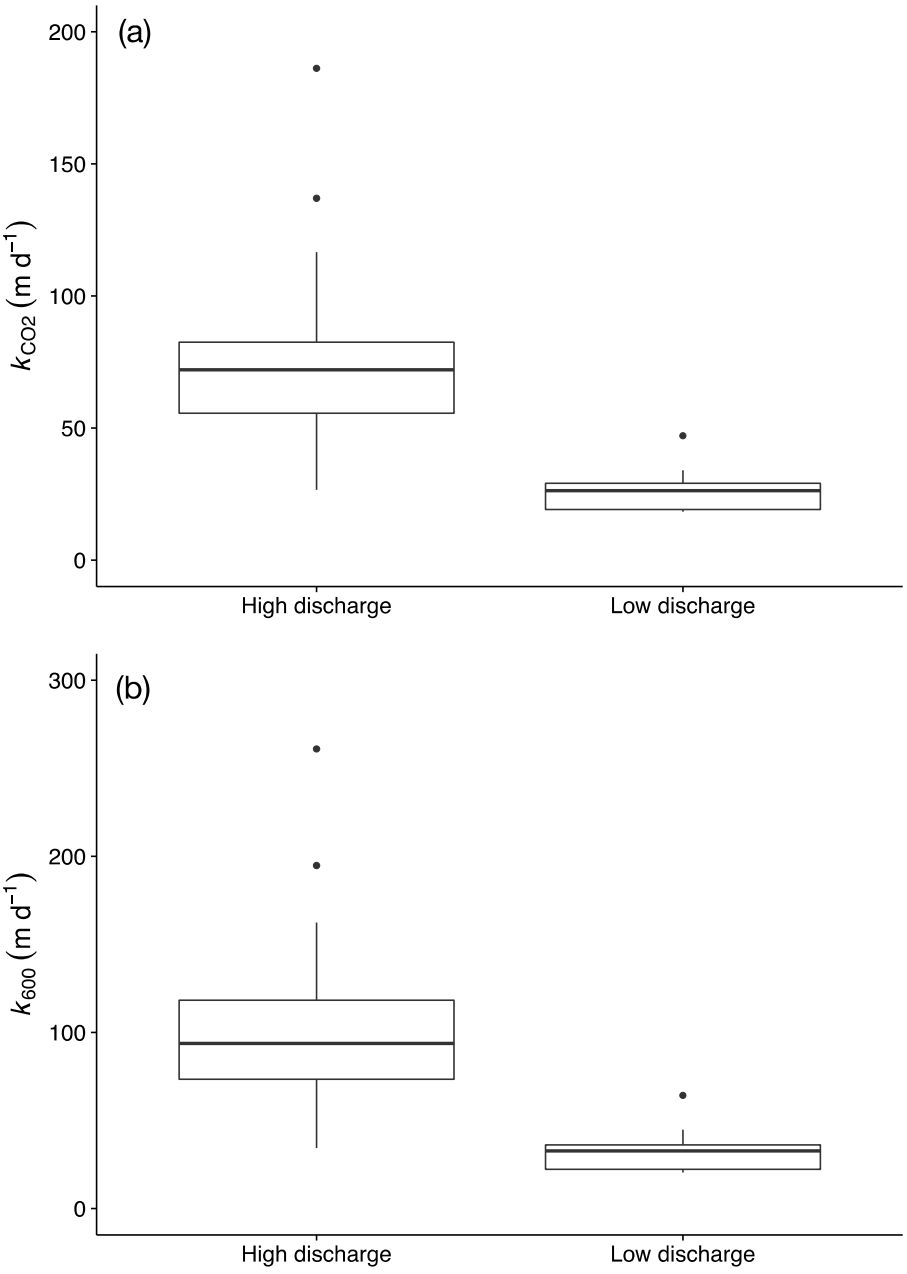

Figure 7. Boxplots of (a) k_{CO2} and (b) k_{600} at low discharge (Q < 100 L s^{-1}) and high discharge (Q > 100 L s^{-1}).

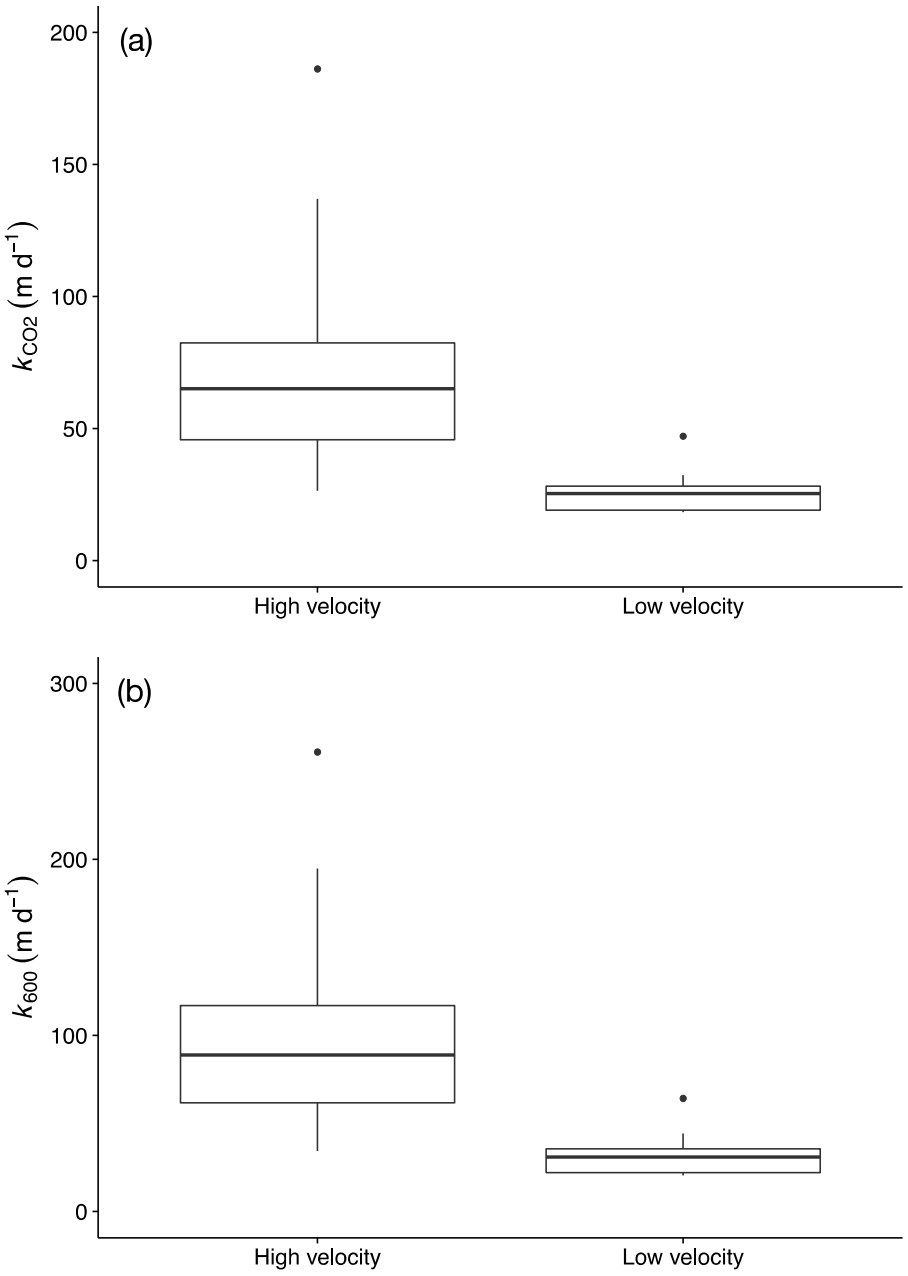

Figure 8. Boxplots of (a) k_{CO2} and (b) k_{600} at low flow velocity (V < 0.13 m s^{-1}) and high flow velocity (V > 0.13 m s^{-1}).

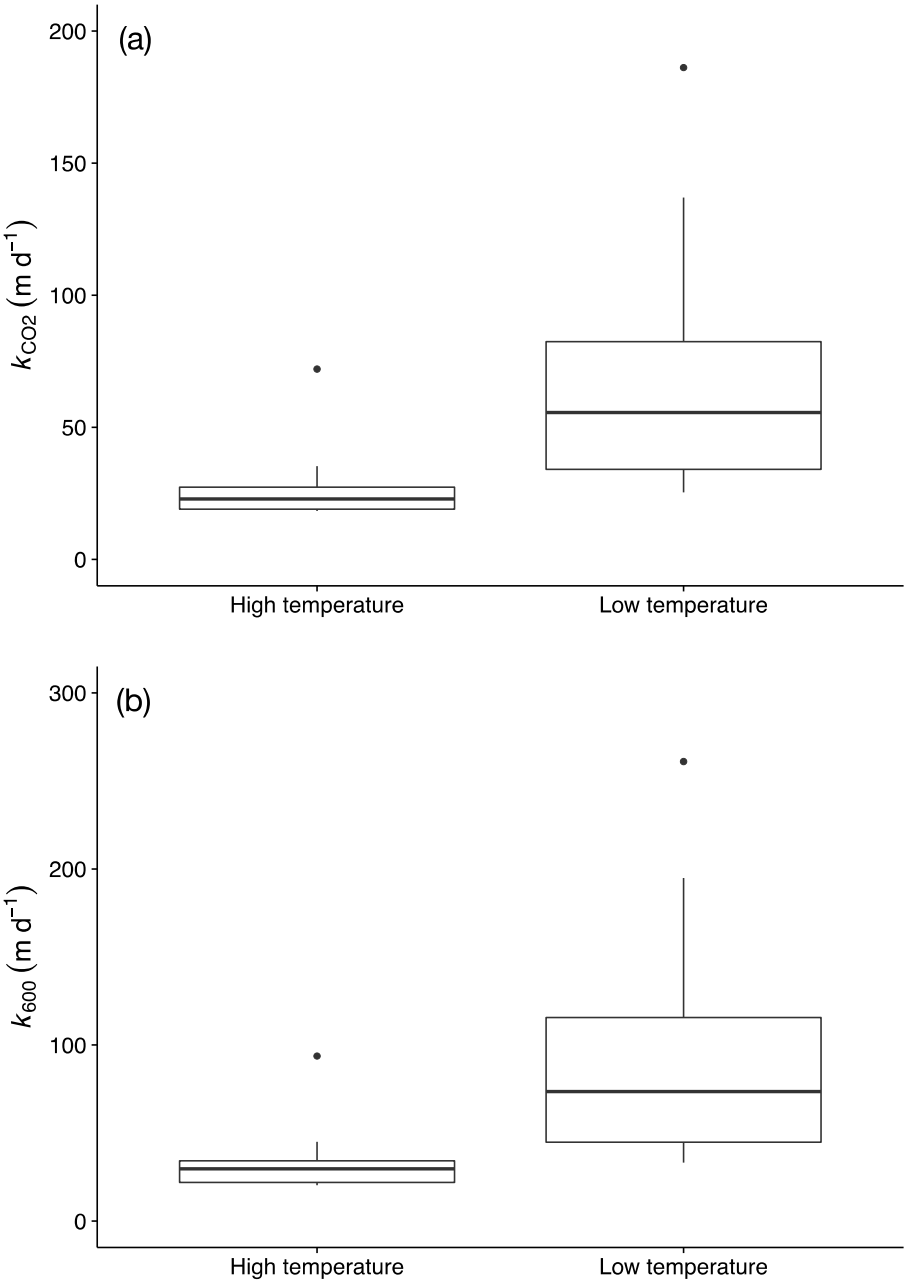

Figure 9. Boxplot of (a) k_{CO2} and (b) k_{600} at low stream temperature (T < 10 ºC) and high stream temperature (T > 10 ºC).

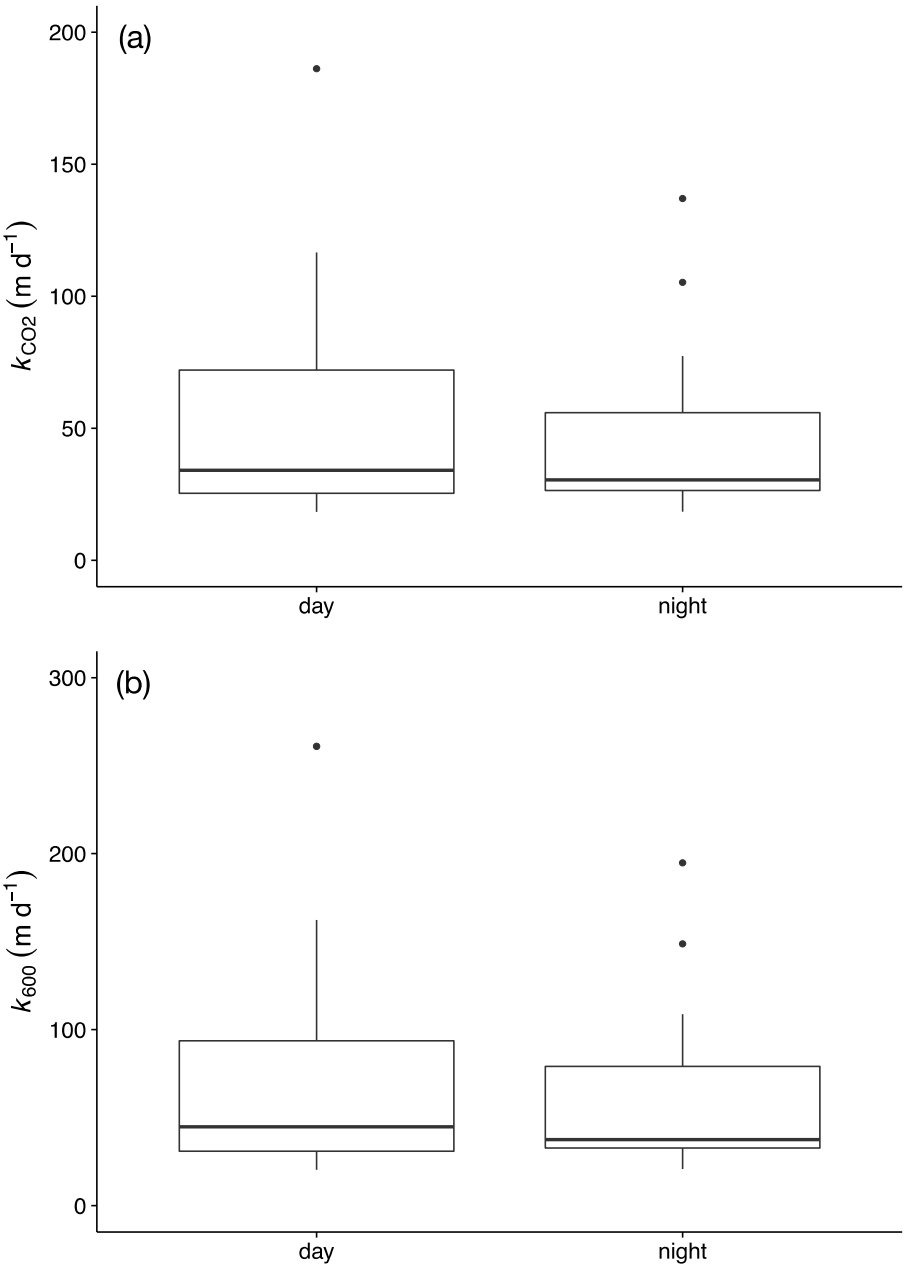

Figure 10. Boxplots of (a) k_{CO2} and (b) k_{600} during daytime and nighttime.

3.3.2 Linear regression models of gas transfer velocities and stream parameters

Linear regression models that predicted log(k_{CO2}) and log(k_{600}) from stream discharge, stream velocity, and stream temperature as single regressor terms performed well, with

discharge having the highest predictive power (r^2 = 0.86 and 0.88; $p < 0.001$ and 0.001), velocity having the second highest (r^2 = 0.82 and 0.85; $p < 0.001$ and 0.001), followed by temperature (r^2 = 0.58 and 0.65; $p < 0.001$ and 0.001). Regression relationships corroborated overall relationships described above, with log(k_{CO2}) and log(k_{600}) positively associated with discharge and velocity and negatively associated with temperature. Figure 11 provides bivariate plots of log(k_{CO2}) and log(k_{600}) and stream discharge, velocity, and temperature, as well as linear regression fits and 95% confidence intervals. Table 9 provides linear regression coefficients and statistics of the six models.

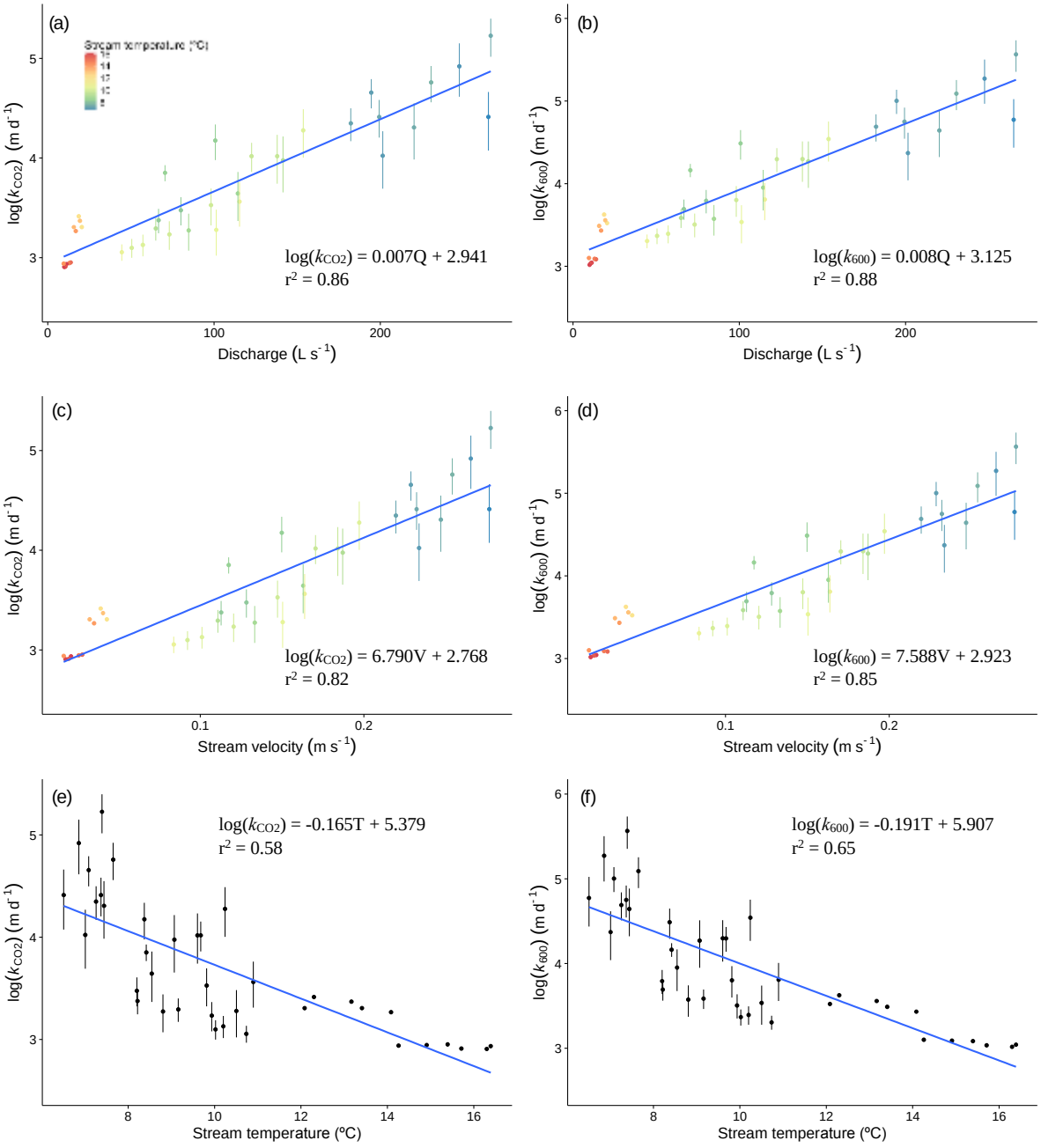

Figure 11. Bivariate plots of (a) log(k_{CO2}) and stream discharge, (b) log(k_{600}) and stream discharge, (c) log(k_{CO2}) and stream velocity, (d) log(k_{600}) and stream velocity, (e) log(k_{CO2}) and stream temperature, and (f) log(k_{600}) and stream temperature (n = 38). Blue lines are linear regression models with equations and coefficients of determination (r^2) given in panel (all p-values < 0.001). Shaded areas are 95% confidence envelopes. Error bars reflect minimum and

maximum pCO_2 measurements considering ±2% IRGA uncertainty (some within the margins of points). Color scale for values and error bars in (a) – (d) indicate stream temperature.

Table 9. Equations, coefficients of determination, residual standard errors (RSE), and p-values of linear regression models that predict log(k_{CO2}) and log(k_{600}) from stream discharge (Q), stream velocity (V), and stream temperature (T) as single regressor terms.

Variable	Equation	r^2	adj. r^2	RSE	p-value
Q	$\log(k_{CO2}) = 0.01Q + 2.94$	0.86	0.85	0.24	< 0.001
V	$\log(k_{CO2}) = 6.79V + 2.77$	0.82	0.81	0.28	< 0.001
T	$\log(k_{CO2}) = -0.16T + 5.38$	0.58	0.57	0.41	< 0.001
Q	$\log(k_{600}) = 0.01Q + 3.12$	0.88	0.87	0.25	< 0.001
V	$\log(k_{600}) = 7.59V + 2.92$	0.85	0.85	0.27	< 0.001
T	$\log(k_{600}) = -0.19T + 5.91$	0.65	0.64	0.41	< 0.001

Multiple linear regression models that predicted log(k_{CO2}) and log(k_{600}) from either stream discharge and temperature or velocity and temperature did not outperform single linear regression models that predicted log(k_{CO2}) and log(k_{600}) from either stream discharge or velocity, with no enhancement of the predictive power of the models by adding a stream temperature term. Stream discharge and temperature had a higher predictive power (r^2 = 0.86 and 0.88; p < 0.001 and 0.001) than stream velocity and temperature (r^2 = 0.82 and 0.85; p < 0.001 and 0.001). Table 10 provides linear regression coefficients and statistics of the four models.

Table 10. Equations, coefficients of determination, residual standard errors (RSE), and p-values of multiple linear regression models that predict log(k_{CO2}) and log(k_{600}) from stream discharge (Q), stream velocity (V), and stream temperature (T) as regressor terms.

Variables	Equation	r^2	adj. r^2	RSE	p-value
Q + T	$\log(k_{CO2}) = 0.01Q - 0.003T + 2.98$	0.86	0.85	0.25	< 0.001
V + T	$\log(k_{CO2}) = 7.92V + 0.04T + 2.24$	0.82	0.81	0.27	< 0.001
Q + T	$\log(k_{600}) = 0.001Q - 0.03T + 3.50$	0.88	0.87	0.25	< 0.001
V + T	$\log(k_{600}) = 7.93V + 0.01T + 2.76$	0.85	0.84	0.27	< 0.001

3.3.3 Model validation of k_{600}

Using empirically determined data for discharge, flow velocity, and stage during CO_2 injections as well as stream slope, I calculated k_{600} from the seven models provided in Raymond et al. (2012). Calculations of k_{600} for each CO_2 injection period estimated by the seven models described by Raymond et al. (2012) yielded mean and median values of 83.8 and 85.0 m d^{-1}, respectively, and range from 12.3 – 172 m d^{-1}. The models overestimated k_{600} compared to measured k_{600} values by 17.8 m d^{-1} on average. Figure 12 illustrates the relationship between measured k_{600} and modeled k_{600}, as well as the linear regression model fit and a 1:1 line. The root mean square error (RMSE) of the model was 29.0 m d^{-1}. Table 11 provides linear regression coefficients and statistics of the model.

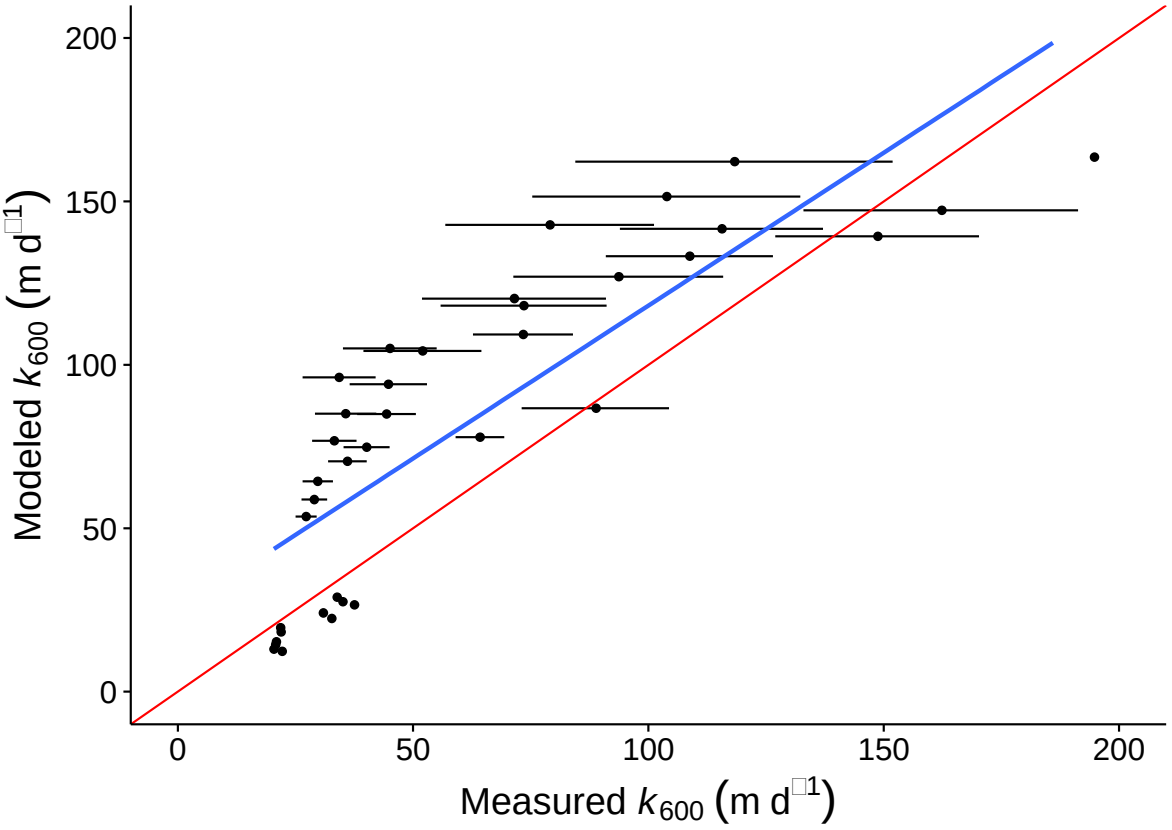

Figure 12. Bivariate plot of measured k_{600} and mean of the modeled k_{600} calculated from seven models described in Raymond et al. (2012) (n = 38). The blue line is a linear regression model with equation: $k_{600\ \text{modeled}} = 0.761 k_{600\ \text{measured}} + 33.541$ ($r^2 = 0.66$, $p < 0.001$). The shaded area is the 95% confidence envelope. The red line is the 1:1 line. Error bars reflect minimum and maximum k_{600} calculations considering ±2% IRGA uncertainty (some within the margins of points).

Table 11. Equation, coefficients of determination, residual standard error (RSE), and p-value of a linear regression model that predicts modeled k_{600} from measured k_{600}.

Equation	r^2	adj. r^2	RSE	p-value
$k_{600\,modeled} = 0.76k_{600\,measured} + 33.54$	0.66	0.65	29.74	< 0.001

3.4 Continuous CO_2 emissions estimates

I computed k_{CO2} and k_{600} on a continuous basis for the study period using the regression relationships between log(k_{CO2}) and log(k_{600}) and discharge (Table 9) and Equations (6) and (7). I also calculated continuous CO_2 emissions (F_{CO2}) from the stream using continuous k_{CO2} and Equation (1). Continuous k_{CO2} and k_{600} reflected variability in continuous discharge, with k_{CO2} and k_{600} exceeding 500 and 900 m d^{-1} on two occasions, during high-flow (Q > 440 L s^{-1}) events (Figure 13). Mean and median k_{CO2} and k_{600} values during the entire study period were 64.6 and 95.1 m d^{-1} and 36.9 and 47.7 m d^{-1}, respectively, and ranged from 20.2 and 24.5 m d^{-1} to 1440 and 2800 m d^{-1}, respectively.

Similarly, continuous CO_2 emissions reflected variability in continuous k_{CO2} and k_{600} and discharge, with the highest fluxes occurring during high flow events with the highest k_{CO2} and k_{600} values discussed above (Figure 13). There was not significant diurnal cycling in k_{CO2} and k_{600} or CO_2 emissions during the study period. Estimated variance in continuous k_{CO2} and k_{600} was very high, with mean and median values of 10700 and 43300 m d^{-1} and 999 and 2270 m d^{-1}, respectively.

A linear regression model that predicted log(F_{CO2}) from continuous stream discharge performed well (r^2 = 0.98, p < 0.001). Similarly, a weighted loess regression model that predicted log(F_{CO2}) from continuous stream velocity performed well (RSE = 0.11). One outlier

(F_{CO2} = 883 g C L^{-1} d^{-1}) was removed to reduce heteroscedasticity and normalize residuals of the loess fit. I found that log(F_{CO2}) was positively associated with flow parameters. Figure 14 provides bivariate plots of log(F_{CO2}) and discharge and flow velocity, as well as regression fits and 95% confidence intervals. Table 12 provides linear regression coefficients and statistics of the linear model. Appendix 4 provides predicted F_{CO2} values of the weighted loess model.

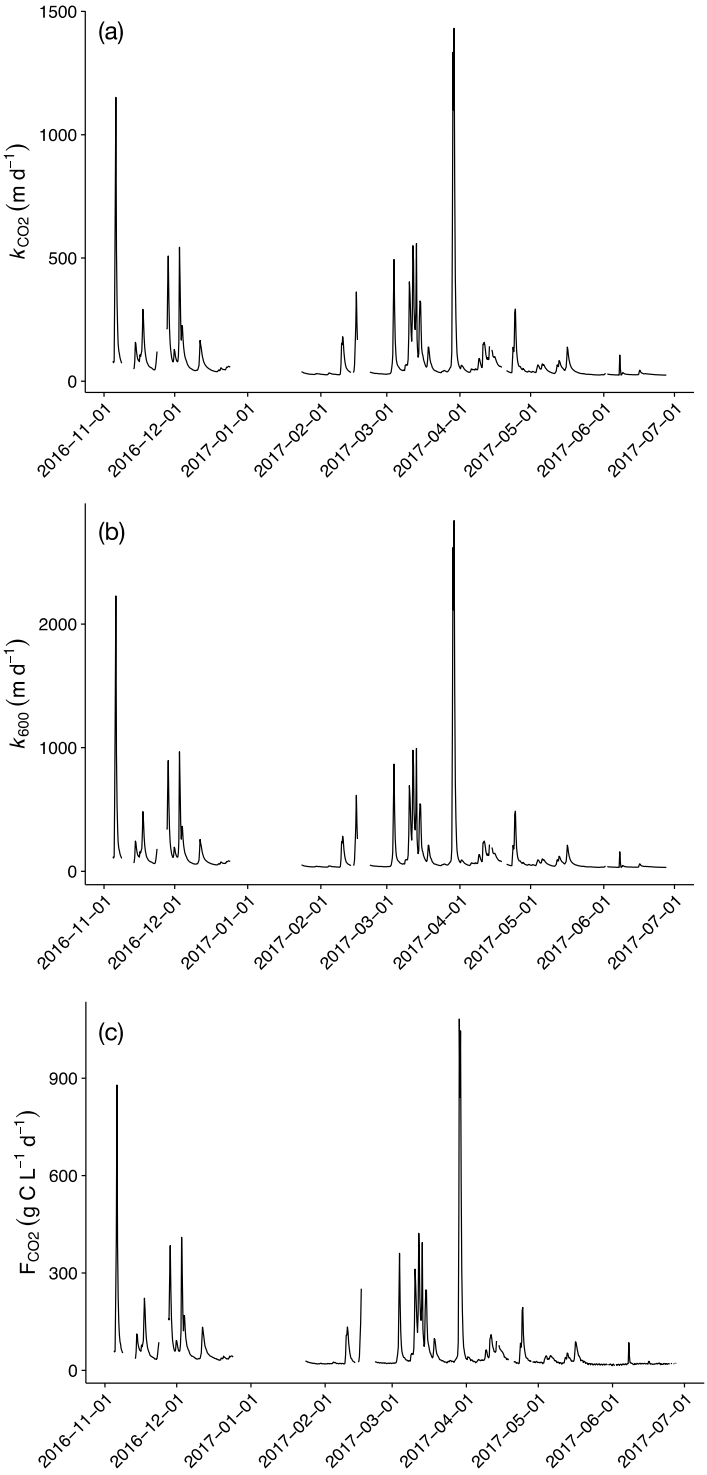

Figure 13. Time series of 6-hour time-averaged (a) k_{CO2}, (b) k_{600}, and (c) CO_2 emissions (F_{CO2}) during the study period.

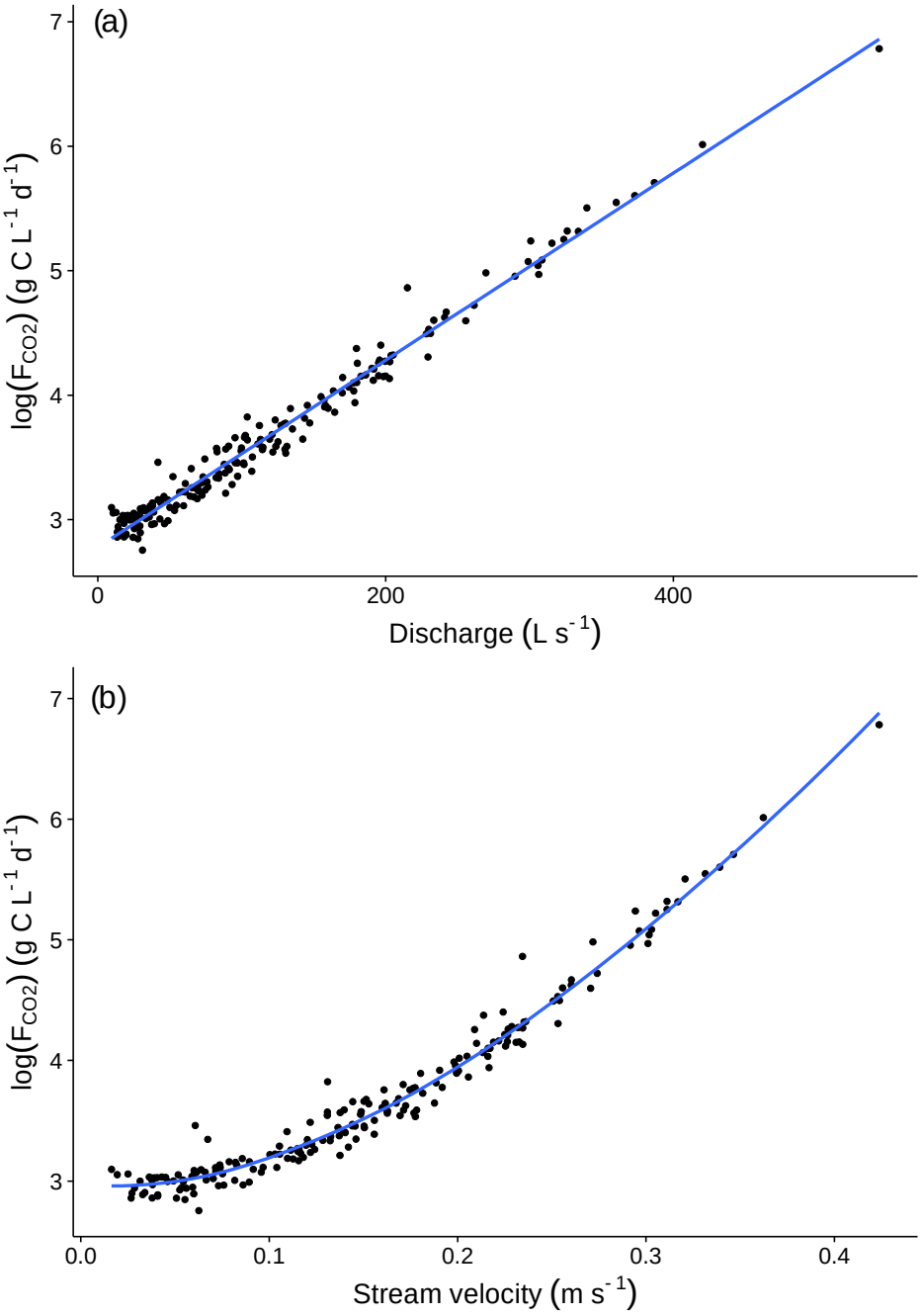

Figure 14. Bivariate plots of (a) continuous discharge (Q) and log(F_{CO2}) and (b) continuous flow velocity and log(F_{CO2}) (n = 194). The blue lines are (a) a linear regression model with equation: log(F_{CO2}) = 0.01Q + 2.58 (r^2 = 0.98; $p < 0.001$) and (b) a loess regression model (RSE = 0.11). The shaded areas are the 95% confidence envelopes.

Table 12. Equation, coefficient of determination, residual standard error (RSE), and p-value of a linear regression model that predicts log(F_{CO2}) from discharge (Q) as a single regressor term.

Variables	Equation	r^2	adj. r^2	RSE	p-value
Q	$\log(F_{CO2}) = 0.01Q + 9.86$	0.97	0.97	0.11	< 0.001

4 DISCUSSION

4.1 Gas transfer velocity estimates

Mean and median k_{600} values were 66.0 and 42.3 m d^{-1}, respectively. These values were in the high range of those reported in the literature, but were in line with those reported for steep, turbulent headwater streams (e.g., Natchimuthu et al., 2017). The mean k_{600} value of the current study was most similar to the mean k_{600} value of 67 m d^{-1} reported in Natchimuthu et al. (2017), a study of CO_2 emissions from the stream network of a forested, hemiboreal catchment in Sweden, in which k_{600} values were determined via propane injections. Streams with very steep reaches and steep waterfalls were included in calculation of this value; excluding the steepest reaches, the mean k_{600} was 6.5 m d^{-1} (Natchimuthu et al., 2017). Average k_{600} values of the present study were also similar to mean and median values of 41.0 and 16.1 m d^{-1} determined via propane injections in 12 peatland headwater streams in the United Kingdom (Billett and Harvey, 2013). A study of O_2 exchange in the Colorado River, Grand Canyon, USA modeled mean k_{600} values of 1410, 37, and 113 m d^{-1} for the rapids, runs, and entire river, respectively (Hall et al., 2012).

The k_{CO2} and k_{600} values determined in the current study also corresponded well with those determined in other streams in the Pacific Northwest (Raymond et al., 2012; Stackpoole

et al., 2012; Stackpoole et al., 2017). A metadata analysis (Raymond et al., 2012) based on five datasets (Bott, 1996; Bott et al., 2006; Melching and Flores, 1999; Mulholland et al., 2001; Tsivoglou and Wallace, 1972) modeled k_{600} values for the Pacific Northwest region of the USA, which ranged from ~25 m d^{-1} to just under 40 m d^{-1}. However, Raymond et al. (2012) cautioned that the models may overestimate k_{600} and are only applicable at large spatial scales.

In a study of aquatic carbon fluxes in five ecoregions of the Western USA, estimated k_{CO2} values for streams in the Western Cordillera, determined via hydraulic relationships, ranged from 10 to 80 m d^{-1} (Stackpoole et al., 2012), and included the models used in the present study (Melching and Flores, 1999; Raymond et al., 2012). In a recent study of riverine and lacustrine gas exchange in multiple regions of Alaska, mean river k_{CO2} values ranged from 9.2 m d^{-1} in the Northwest region to 27.5 m d^{-1} in the Southeast region, with a mean value for all regions of 14.6 m d^{-1} (Stackpoole et al., 2017).

The range of k_{600} values reported in the present study (20.4 – 261 m d^{-1}) were also within the range of, and in some cases much lower than, the upper range of k_{600} values reported in the literature. A study of gas exchange in the Amazon and Mekong river systems reported k_{600} values determined using floating chambers for streams and small rivers (<100 m wide) as high as 71 m d^{-1} (Alin et al., 2011). Hall and Tank (2003) reported an upper range for k_{600} of 42 m d^{-1} determined via SF_6 injections in small streams in Grand Teton National Park, Wyoming. Upper ranges for k_{600} in rapids, runs, and the entire river system in the Colorado River, Grand Canyon, USA were 7730, 143, and 113 m d^{-1}, respectively (Hall et al., 2012). Natchimuthu et al. (2017) determined an upper range of 558.7 m d^{-1} in the steepest reaches of headwater streams in a Swedish hemiboreal catchment.

However, many previous studies have reported average k_{600} values for headwater streams and small rivers lower than the range of those determined in the present study. Butman and Raymond (2011) estimated a mean k_{600} value of 18 m d^{-1} based on a model using slope and flow velocity terms in the steep headwater streams of the American west. Hall and Tank (2003) determined a mean k_{600} value of 18.4 m d^{-1} in the small streams of Grand Teton National Park, Wyoming, USA. Wallin et al. (2011) determined mean and median k_{600} values of 13 and 7.4 m d^{-1}, respectively, via propane injections in boreal headwater streams in Sweden. Mean and median k_{600} values for a first-order stream in Walker Branch, Tennessee, USA determined via propane injections were 5 and 7 m d^{-1}, respectively (Wanninkhof et al., 1990), and ranged from 5.5 – 14.2 m d^{-1} (Roberts et al., 2007). Streams and small rivers (<100 m wide) in the Amazon and Mekong river systems yielded a mean k_{600} value of 5.6 m d^{-1} (Alin et al., 2011). Campeau et al. (2014) determined k_{600} values for a lowland boreal river system in Northern Quebec using suspended floating chambers and corroborated results with modeled values; the mean of all samples (stream orders 1 – 6) was under 1 m d^{-1}, with lower orders having the lowest mean k_{600} values. Crawford et al. (2013) determined a mean value of 6.5 m d^{-1} for a boreal headwater stream network in Alaska using suspended floating chambers. The mean and range values of k_{600} for five small streams in the Northern Highlands Lake District of north central Wisconsin and Michigan, USA, determined via suspended floating chambers, were 3.9 m d^{-1} and 0.3 – 13.5 m d^{-1}, respectively (Crawford et al., 2014). A mean k_{600} value for first-order streams in Sweden determined via equations with slope and depth parameters (O'Connor and Dobbins, 1958) was 6.5 m d^{-1} (Humborg et al., 2010). In a study of CO_2 emissions from low-gradient (<4%) streams in a southwestern Alaskan watershed, Smits (2016) estimated a

mean k_{600} value of 5.9 m d^{-1} from an oxygen-based regression model, and 6 m d^{-1} from the models used in the present study.

Thus, k_{600} values determined in the present study were in the high range of, and in some cases much higher than, reported k_{600} values for streams and rivers in general, and headwater streams specifically. Billett and Harvey (2013) discussed potential reasons why their k_{600} estimates were higher than those previously published for headwater streams, noting that multiple measurements were conducted during high discharge events, and that the reaches they used were narrower and deeper than those used in other studies, with stream width to depth ratios ranging from 2 to 15. In the present study, mean discharge observed during CO_2 injection periods ranged from 10 to 266 L s^{-1}, with mean and median values of 101 and 82 L s^{-1}, respectively. Mean and median discharge values observed during the entire study period were 117 and 93 L s^{-1}, respectively, and ranged from 9 to 601 L s^{-1}. Average k_{600} values therefore represent and likely slightly underestimate k_{600} values for the entire study period, with the range of k_{600} values excluding very high flow events. The mean stream width to depth ratio observed during CO_2 injections was 19, which is higher than those observed in Billett and Harvey (2013), but lower than those observed in other studies (e.g., Hall and Tank, 2003).

There was good correspondence between modeled k_{600} values and measured k_{600} values, with a linear regression model using measured k_{600} as an external regressor explaining 66% of the variance in modeled values. This is slightly higher than the predictive power of the models in the original metadata analysis (mean $r^2 = 0.63$) (Raymond et al., 2012). In the present study, models overestimated k_{600} by 17.8 m d^{-1} on average, which is generally consistent with conclusions of the original analysis (Raymond et al., 2012). The original analysis also found

that k_{600} values were generally highest in headwater streams in the Pacific Northwest region, compared to all other regions of the USA (Raymond et al., 2012).

In a study of gas exchange in a hemiboreal headwater stream network, Natchimuthu et al. (2017) found that the models for k_{600} performed well for values below 100 m d^{-1} but underestimated values above 100 m d^{-1} by as much as 80%, likely because the models were not developed in the context of reaches with steep slopes or high altitudes and correspondingly high k_{600} values (Natchimuthu et al., 2017; Raymond et al., 2012; Stackpoole et al., 2012). In the present study, models underestimated k_{600} for values above 139 m d^{-1}. The slope of this reach (13.3º, equivalent to 23.6% slope) was slightly higher than the highest slope category (6 – 21%) studied in Natchimuthu et al. (2017), which the authors found to generate the highest k_{600} values. A high slope for this reach may therefore explain both generally high k_{600} values and model performance. Other studies have noted that slope is positively associated with k_{600} (Moog and Jirka, 1999; Raymond et al., 2012), although some studies have reported no correspondence between slope and k_{600} (e.g., Smits, 2016).

4.2 Relationships between gas transfer velocities and stream parameters

I found good correspondence between k_{CO2} and k_{600} and stream discharge, velocity, and temperature, with single linear regression models using these parameters as external regressors explaining 86 and 88%, 82 and 85%, and 58 and 65% of the variance in k_{CO2} and k_{600}, respectively. Values for k_{CO2} and k_{600} were positively associated with discharge and flow velocity, and negatively associated with stream temperature. Boxplots of k_{CO2} and k_{600} at high and low values of stream discharge, velocity, and temperature illustrate these relationships (Figures 12 – 17).

Previous studies have found good correspondence between k_{600} and discharge (e.g., Natchimuthu et al., 2017), but the relationship is generally spatiotemporally variable (Billett and Harvey, 2013; Wallin et al., 2011) and depends on the relationship between discharge and turbulence in a given reach (Wallin et al., 2011). Gas exchange studies that have determined k_{600} for multiple reaches in a catchment under multiple flow conditions have found positive, negative, and zero correspondence between k_{600} and discharge in different reaches (Billett and Harvey, 2013; Natchimuthu et al., 2017; Wallin et al., 2011). Two studies that determined k_{600} for different reaches in the same stream found positive (Roberts et al., 2007) and zero (Genereux and Hemond, 1992) correspondence between k_{600} and discharge. Natchimuthu et al. (2017) found that the correspondence between k_{600} and discharge increased positively with increasing slope, suggesting that steeper reaches generate more turbulence with higher flow than flatter reaches, thereby increasing gas evasion (Wallin et al., 2011). This reach was relatively steep compared to previously studied reaches and generated turbulence in many areas under high flow conditions, which may explain the strong relationships between k_{CO2} and k_{600} and mean discharge. Correspondingly, many studies have found both a strong positive relationship (Billett and Harvey, 2013; Natchimuthu et al., 2017; Sand-Jensen and Staehr, 2012) and no relationship (Natchimuthu et al., 2017) between flow velocity and k_{600}. Variable channel morphologies and bed characteristics in a given catchment therefore limit the potential for regional scaling of k_{600} based on discharge or flow velocity terms (Moog and Jirka, 1999; Wallin et al., 2011).

Additionally, previous work comparing studies from different latitudes has shown that k_{600} varies with stream temperature, although the predictor is not as strong as turbulence parameters (Aufdenkampe et al., 2011). Similarly, the present study shows that k_{CO2} and k_{600}

were negatively associated with stream temperature, but the parameter explains less of the variance in k_{CO2} and k_{600} (58 and 65%) than discharge and velocity as single regressor terms. Water temperature may be a strong predictor for k_{600} in lakes, where convection at the air-water interface drives turbulence (Holgerson et al., 2017; MacIntyre et al., 2010). In streams, streamflow and morphological parameters drive turbulence, rather than convection (Wallin et al., 2011). Figure 11 indicates that stream temperature was strongly associated with discharge and velocity in the present study, suggesting that the relationship between stream temperature and k_{CO2} and k_{600} was due to the strong seasonal relationship between stream temperature and flow parameters. Further, k_{CO2} values calculated using mean pCO_2, travel time, and stage parameters from CO_2 injections showed no change with changing temperature, given that all other parameters stayed the same and temperature values from both sensors changed concurrently. Under these conditions, k_{600} values decreased with increasing stream temperature (e.g., by 4 m d^{-1} between 6 and 8ºC).

4.3 CO_2 evasion estimates

CO_2 evasion from headwater streams has been reported as the dominant process governing aqueous C fluxes in a boreal landscape (Wallin et al., 2013). Studies have reported high spatiotemporal variability in both stream pCO_2 and CO_2 emissions from headwater streams (Billett and Harvey, 2013; Sand-Jensen and Staehr, 2012; Wallin et al., 2013), with variability in gas transfer velocities controlling CO_2 evasion (Wallin et al., 2011) and decreasing pCO_2 with increasing gas transfer velocities (Dosch, 2014). Additionally, pCO_2 decreases and CO_2 evasion increases with increasing slope in headwater streams (Finlay, 2003; Natchimuthu et al., 2017; Wallin et al., 2011). Wallin et al. (2011) found that stream slope,

width, and depth parameters explained 83% of spatial variability in gas transfer velocities in a boreal stream network. In a hemiboreal headwater catchment, Natchimuthu et al. (2017) determined that the steepest slope category (6 – 21%) generated CO_2 emissions four times greater than the mean emissions for all studied reaches, despite comprising 0.9% of the total stream surface area. The authors further hypothesized that high flow events in steep headwater streams may play a dominant role in annual CO_2 emissions from a catchment, even if they occur over short periods of time (Natchimuthu et al., 2017).

In the present study, CO_2 emissions were variable overall and highest during high flow events, with discharge explaining 97% of the variability in emissions and flow velocity explaining 89% of the variability in emissions during the study period. High flow events were likely "hot moments" of CO_2 evasion (McClain et al., 2003); almost 80% of CO_2 emissions occurred when discharge was greater than the median overall discharge of 92 L s^{-1}. The high slope, high gas transfer velocities, and high degree of turbulence in this stream suggest that it may play an important role in CO_2 emissions from the catchment, with future climate-driven hydrological regime changes potentially increasing current emissions estimates (Natchimuthu et al., 2017). Additionally, estimates of CO_2 evasion calculated using k_{600} determined via the seven models used in the present study underestimated CO_2 evasion by a mean of 1191 g C L^{-1} d^{-1}, corroborating evidence that high flow events are significant determinants of CO_2 evasion from headwater streams and are likely underrepresented by infrequent measurements and modeled calculations. Figure 15 provides a comparison of modeled CO_2 evasion over the study period from the two methods; evasion calculated using k_{600} determined via the seven models used in the present study again underrepresented the highest modeled flux events. An important note is that CO_2 evasion estimates were determined from back-transformed logarithmic

estimates of continuous k_{CO2}, which had very high calculated uncertainties, in some cases higher than k_{CO2} estimates by multiple orders of magnitude. Thus, modeling k_{CO2} and k_{600} or F_{CO2} in this way may not be reliable, depending on the desired accuracy of the estimates.

4.4 Advantages and drawbacks of automated CO_2 injections as a tracer for k_{CO2} and F_{CO2}

Despite the widespread use of tracer gas injections for determining gas transfer velocities, shortcomings of current techniques result in analytical variability (Sand-Jensen and Staehr, 2012) and data scarcity (Marx et al., 2017). Sand-Jensen and Staehr (2012) provide a comprehensive discussion regarding limitations of using tracer gases (e.g. oxygen, propane, ethane, SF_6) in aqueous CO_2 emissions studies, including errors associated with Schmidt conversions (Cole and Caraco, 1998; Simonsen, 1974; Thyssen and Kelly, 1985), pH-dependent conversions of CO_2 in aqueous environments (Ho et al., 1997), and differences in how different gases pass through an organic-rich air-water interface (Frew, 1997).

Conventional tracer gas studies also rely on manual sampling, which limits the frequency and timing with which samples can be collected. For example, there is a paucity of nighttime gas exchange data collected via tracer gas analysis (Marx et al., 2017), despite the likelihood that diurnal processes, such as in-stream metabolism (Crawford et al., 2013), affect gas transfer velocities and CO_2 emissions (Schelker et al., 2017). In a study of CO_2 evasion from a steep, high gradient stream network in the European Alps, evasion was highest at nighttime and lowest at daytime (Schelker et al., 2017). However, in a study of CO_2 evasion from a large boreal river in Finland, Huotari et al. (2013) reported no significant diurnal cycling in CO_2 fluxes. Similarly, in the present study, there were no significant diurnal trends in gas transfer velocities or CO_2 fluxes. This finding is likely supported by the hypothesis that most

streamwater CO_2 is terrestrially-derived (Dinsmore and Billett, 2008; Hope et al., 2004), and thus stream pCO_2 was largely not governed by in-stream processes during the present study. However, year-round data collection as streamflow permits will allow for a better interpretation of the importance of in-stream processes for CO_2 evasion dynamics. Continued research on diurnal trends in CO_2 transfer velocities and emissions will elucidate processes and fill in data gaps. Additionally, it is worth noting that innovations in tracer gas techniques have incorporated diurnal sampling; for example, Tobias et al. (2009) measured gas transfer continuously for 32 hours by pumping dilute SF_6-saturated water into a stream.

While methods that include direct measurements of CO_2 fluxes, such as floating chamber techniques, can be deployed for extended periods of time and preclude analytical errors associated with conventional tracer gas studies, they have been criticized for underestimating fluxes by disrupting turbulence and creating artificial pressure and temperature conditions (Gafalk et al., 2013; Crawford et al., 2014; Raymond and Cole, 2001). Suspended chamber techniques have mitigated some of these effects and validated data with other methods (Crawford et al., 2013; Crawford et al., 2014).

Direct injection of CO_2 for use as a tracer precludes analytical variability concerning Schmidt conversions, pH dependencies, and gas-dependent interactions at the air-water interface. *In situ* measurement of pCO_2 also has advantages over *ex situ* measurement (e.g. systems that circulate air to a sensor outside of the stream), including enhanced precision and response time (Johnson et al., 2010). Further, automated injections allow for continuous monitoring at any desired time scale. Although trigger parameters for automated injections other than time of day were not tested in the present study, it is certainly possible to program a datalogger to collect tracer data in response to events of scientific interest, given that other

sensors connected to the datalogger are measuring ancillary variables. For example, a future direction of the present study may be to trigger CO_2 injections during high-flow events by setting a threshold for stream depth.

Previous studies have tested the IRGA sensors used in the present study for output stability and long-term drift during continuous deployment in both streamwater (Johnson et al., 2010) and soil (Jassal et al., 2004) environments. Additionally, the sensors have exhibited output stability in a wide range of aqueous environments and have not required data cleaning (Johnson et al., 2010).

However, the experimental setup, including automated CO_2 injections, has some disadvantages and may not be suitable for every field campaign. Researchers working in sites with public access should consider the possibility of equipment being tampered with, which can result in expensive losses, for example in the case of sensors being broken or stolen. Further, compressed gas cylinders may need to be replaced frequently and can also pose a safety hazard for inexperienced users and curious wildlife, such as bears. Gas cylinders should be covered properly, ideally in a locked container. Additionally, negative and positive outliers in the present study may have been due to inadequate gas mixing in the reach or sensor malfunction.

4.5 Considerations

In general, I overestimated gas injection times that were needed for sensor equilibration, especially during winter months when stream discharge and flow velocity were high. In response, I manually adjusted gas flow rates as necessary during field visits in response to changing streamflow and stream temperature. Future experimental deployments using this method will benefit from adjusting gas flow and injection time based on the dynamics of

specific stream reaches. To further automate this method, researchers may wish to include streamflow and temperature thresholds in their datalogger programs that govern injection times and gas flow rates based on determined stream dynamics.

Another consideration is the potential influence of hyporheic exchange on evasion estimates in headwater stream systems. While hyporheic exchange likely does not significantly affect estimates during high flow conditions (Leach and Moore, 2014), it may play a larger role during lower flow conditions by impacting pCO_2 and promoting evasion. CO_2 generation in the hyporheic zone and efflux rates may be significant in streams (Schindler and Krabbenhoft, 1998); in the Pacific Northwest, hyporheic zone pCO_2 has been shown to be highest during the summer and lowest during the winter, with winter storms quickly decreasing and subsequently increasing hyporheic zone pCO_2 (Brandes, 2017).

The presence of hyporheic exchange pathways can be determined by frequently monitoring pCO_2 at many points in the study reach during various flow conditions, and particularly in response to high flow events. Nevertheless, its influence on evasion estimates should be mitigated through a long gas injection period during which sufficient time is provided for sensor equilibration.

Additionally, comparison of discharge estimates from upstream and downstream sensor locations during salt slug injections indicated that study reach was generally a gaining reach. Thus, larger-scale hydraulic forcing conditions may affect evasion estimates, perhaps more than hyporheic exchange, particularly as the losing or gaining flux increases (Fox et al., 2014).

It is also worth noting that significantly elevating pCO_2 in an aqueous environment for long periods of time may have impacts on ecosystems by decreasing pH, resulting in litter and

algal quality decreases and food web effects (Ferreira and Chauvet, 2011; Hargrave et al., 2009). However, elevated pCO_2 may also increase the density, biomass, and average individual size of benthic invertebrates (Hargrave et al., 2009). Further, although studies have focused on simulating potential climate change scenarios in streams by elevating pCO_2 for long periods of time (e.g., 90 days), no study to my knowledge has looked at long-term effects of elevating aqueous pCO_2 for short bursts (e.g., 1 hour twice per day). Additionally, in turbulent headwater streams particularly, all injected CO_2 will likely evade within a confined reach, although there is a possibility that some is taken up by an ecosystem. More research may be needed to ensure that this method does not harm stream ecosystems, and site-specific evasion dynamics should be taken into consideration. One complementary path for this research may be isotopic analysis of CO_2 during baseline conditions and CO_2 injections, which could help discriminate among various CO_2 pathways.

5 CONCLUSIONS

The limitations of current methods for determining gas transfer velocities of CO_2 in headwater streams result in analytical variability and data scarcity. The method presented here mitigates common issues associated with gas transfer velocity estimations. The use of CO_2 as a tracer precludes analytical variability associated with the use of alternative gases while maintaining natural conditions at the air-water interface, and automated injections allow researchers to determine gas transfer velocities at the desired temporal scale. In the present study, k_{CO2} and k_{600} showed good correspondence with stream discharge, velocity, and temperature, with correspondence decreasing in that order. Values of k_{CO2} and k_{600} associated positively with both discharge and flow velocity and negatively with stream temperature;

continuous k_{CO2} and k_{600} extrapolation indicated that the highest k_{CO2} and k_{600} values occurred during very high flow events, when turbulence was highest. Values of k_{600} were generally high but within the range of those reported in previous studies; high k_{600} values also corresponded well with stream morphological and turbulence parameters. Similar to other studies in steep headwater streams, k_{600} values determined via seven widely-used models performed well for values under 139 m d^{-1} but underestimated k_{600} above this threshold, suggesting that the models were not developed for steep headwater streams under high flow conditions. CO_2 emissions estimates suggested that high flow conditions drove evasion during the study period and may become more important if climate-driven hydrological regime changes result in more frequent high flow events. Constraining estimates of CO_2 evasion from headwater streams is a critical step in characterizing the global carbon cycle. The method presented in this thesis will allow researchers to increase the frequency and accuracy with which they can determine gas transfer velocities of CO_2 in headwater streams, ultimately resulting in data-driven quantifications of CO_2 emissions and fluxes in the global C cycle.

REFERENCES

Alin, S. R., M. D. D. F. F. L. Rasera, C. I. Salimon, J. E. Richey, G. W. Holtgrieve, A. V. Krusche, and A. Snidvongs (2011), Physical controls on carbon dioxide transfer velocity and flux in low-gradient river systems and implications for regional carbon budgets, *J. Geophys. Res., 116*(G1), doi:10.1029/2010JG001398.

Aufdenkampe, A. K., E. Mayorga, P. A. Raymond, J. M. Melack, S. C. Doney, S. R. Alin, R. E. Aalto, and K. Yoo (2011), Riverine coupling of biogeochemical cycles between land, oceans, and atmosphere, *Front. Ecol. Environ., 9*(1), 53–60, doi:10.1890/100014.

Baskerville, G. L. (1972), Use of Logarithmic Regression in the Estimation of Plant Biomass, *Canadian Journal of Forestry 2*(49), 49–53, doi:10.1139/x72-009.

Battin, T. J., S. Luyssaert, L. A. Kaplan, A. K. Aufdenkampe, A. Richter, and L. J. Tranvik (2009), The boundless carbon cycle, *Nat. Geosci., 2*, 598–600, doi:10.1038/ngeo618

Benstead, J. P., and D. S. Leigh (2012), An expanded role for river networks, *Nat. Geosci., 5*, 678–679, doi:10.1038/ngeo1593.

Billett, M. F., and F. H. Harvey (2013), Measurements of CO_2 and CH_4 evasion from UK peatland headwater streams, *Biogeochemistry, 114*, 165–181 doi:10.1007/s10533-012-9798-9.

Bott, T. L, (1996), Primary productivity and community respiration, *Methods in Stream Ecology. Academic Press, San Diego, California*, 533–556.

Bott, T. L., D. S. Montgomery, J. D. Newbold, D. B. Arscott, C. L. Dow, A. K. Aufdenkampe, J. K. Jackson, and L. A. Kaplan (2006), Ecosystem metabolism in streams of the Catskill Mountains (Delaware and Hudson River watersheds) and lower Hudson Valley, *J. N. Am. Benthol. Soc., 25*(4), 1018–1044, doi:10.1899 /0887-3593(2006)025[1018:EMISOT]2.0.CO;2.

Brandes, J. B. (2017), The vadose zone as a hyporheic carbon source: a look at temporal trends in hyporheic zone pCO_2, M.Sc. thesis, Oregon State University, Corvallis.

Butman, D., and P. A. Raymond (2011), Significant efflux of carbon dioxide from streams and rivers in the United States, *Nat. Geosci., 4*, 839–842, doi:10.1038/ngeo1294.

Campeau, A., J.-F. Lapierre, D. Vachon, and P. A. del Giorgio (2014), Regional contribution of CO_2 and CH_4 fluxes from the fluvial network in a lowland boreal landscape of Québec, *Global Biogeochem. Cycles, 28*(1), 57–69, doi:10.1002/2013GB004685.

Clark, J. F., P. Schlosser, H. J. Simpson, M. Stute, R. Wanninkhof, and D. T. Ho (1995), Relationship between gas transfer velocities and wind speeds in the tidal Hudson River determined by the dual tracer technique, *Air-water gas transfer*, 785-800.

Cole, J. J., et al. (2007), Plumbing the global carbon cycle: Integrating inland waters into the terrestrial carbon budget, *Ecosystems, 10*(1), 171–184, doi:10.1007/s10021-006-9013-8.

Cole, J. J., and N. F. Caraco (1998), Atmospheric exchange of carbon dioxide in a low-wind oligotrophic lake measured by the addition of SF_6, *Limnol. Oceanogr., 43*(4), 647–656.

Crawford, J. T., N. R. Lottig, E. H. Stanley, J. F. Walker, P. C. Hanson, J. C. Finlay, and R. G. Striegl (2014), CO_2 and CH_4 emissions from streams in a lake-rich landscape: Patterns, controls, and regional significance, *Global Biogeochem. Cycles, 28*(3), 197–210, doi:10.1002/2013GB004661.

Crawford, J. T., R. G. Striegl, K. P. Wickland, M. M. Dornblaser, and E. H. Stanley (2013), Emissions of carbon dioxide and methane from a headwater stream network of interior Alaska, *J. Geophys. Res., 118*(2), 482–494, doi:10.1002/jgrg.20034.

Dinsmore, K. J., and M. F. Billett (2008), Continuous measurement and modelling of CO2 losses from a peatland stream during stormflow events, *Water Resour. Res., 44*(12), W12417, doi:10.1029/2007WR007284.

Dosch, N. T. (2014), Spatiotemporal Dynamics and Drivers of Stream pCO2 in a Headwater Catchment in the Western Cascade Mountains, Oregon, M.Sc. thesis, Oregon State University, Corvallis.

Ferreira, V., and E. Chauvet (2011), Future increase in temperature more than decrease in litter quality can affect microbial litter decomposition in streams, *Oecologia, 167*, 279–291, doi:10.1007/S00442-01 1-1976-2

Finlay, J. C. (2003), Controls of streamwater dissolved inorganic carbon dynamics in a forested watershed, *Biogeochemistry, 62*(3), 231-252.

Fox, A., F. Boano, and S. Arnon (2014), Impact of losing and gaining streamflow conditions on hyporheic exchange fluxes induced by dune-shaped bed forms, *Water Resour. Res., 50*(3), 1895–1907, doi:10.1002/2013WR014668

Frankignoulle, M., G. Abril, A. Borges, I. Bourge, C. Canon, B. DeLille, E. Libert, and J. M. Theate (1998), Carbon dioxide emission from European estuaries, *Science, 282*(5388), 434–436, doi:10.1126/science.282.5388.434

Frew, N.M. (1997), The role of organic films in air-sea gas exchange. *The sea surface and global change*, edited by P. S. Liss, and R. A. Duce, 121–163.

Gafalk, M., D. Bastviken, S. T. Fredriksson, and L. Arneborg (2013), Determination of the piston velocity for water-air interfaces using flux chambers, acoustic Doppler velocimetry, and IR imaging of the water surface, *J. Geophys. Res.: Biogeosciences, 118*(2), 770-782.

Genereux, D. P., and H. F. Hemond (1992), Determination of Gas-Exchange Rate Constants for a Small Stream on Walker Branch Watershed, Tennessee, *Water Resour. Res., 28*(9), 2365-2374.

Gibs, J., F. D. Wilde, and H. A. Heckathorn (2007), Use of Multiparameter Instruments for Routine Field Measurements, *U.S. Geological Survey Techniques of Water-Resources Investigations* (Book 9, Chapter A6, Section 6.8).

Gomi, T., R. C. Sidle, and J. S. Richardson (2002), Understanding processes and downstream linkages of headwater systems, *BioScience, 52*(10), 905–916.

Hall, R. O., T. A. Kennedy, and E. J. Rosi-Marshall, Air–water oxygen exchange in a large whitewater river (2012), *Limnol. Oceanogr.: Fluids Environ. 2*(1), 1–11, doi: 10.1215/21573689-1572535.

Hall, R. O., and J. L. Tank (2003), Ecosystem metabolism controls nitrogen uptake in streams in Grand Teton National Park, Wyoming, *Limnol. Oceanogr., 48*(3), 1120–1128, doi: 10.4319/lo.2003.48.3.1120

Hargrave, C. W., K. P. Gary, and S. K. Rosado (2009), Potential effects of elevated atmospheric carbon dioxide on benthic autotrophs and consumers in stream ecosystems: a test using experimental stream mesocosms, *Global Change Biology*, *15*(11), 2779–2790, doi:10.1111/j.1365-2486.2009.01897.x.

Ho, D.T., L. F. Bliven, R. Wanninkhof, and P. Schlosser (1997), The effect of rain on air-water gas exchange, *Tellus, 49*(2), 149–158, doi: 10.1034/j.1600-0889.49.issue2.3.x

Holgerson, M. A., E. R. Farr, and P. A. Raymond (2017), Gas transfer velocities in small forested ponds, *J. Geophys. Res. Biogeosci., 122*, 1011–1021, doi:10.1002/2016JG003734.

Hope, D., S. M. Palmer, M. F. Billett, and J. J. C. Dawson (2001), Carbon dioxide and methane evasion from a temperate peatland stream, *Limnol. Oceanogr., 46*(4), 847–857, doi: 10.4319/lo.2001.46.4.0847

Hope, D., S. M. Palmer, M. F. Billett, and J. J. C. Dawson (2004), Variations in dissolved CO_2 and CH_4 in a first-order stream and catchment: An investigation of soil-stream linkages, *Hydrol. Process., 18*(17), 3255–3275, doi:10.1002/hyp.5657.

Humborg, C., C. M. Mörth, M. Sundbom, H. Borg, T. Blenckner, R. Giesler, and V. Ittekkot (2010), CO_2 supersaturation along the aquatic conduit in Swedish watersheds as constrained by terrestrial respiration, aquatic respiration and weathering, *Global Change Biol., 16*(7), 1966–1978, doi:10.1111/j.1365-2486.2009.02092.x.

Huotari, J., S. Haapanala, J. Pumpanen, T. Vesala, and A. Ojala (2013), Efficient gas exchange between a boreal river and the atmosphere, *Geophys. Res. Lett.,40*(21), 5683–5686, doi:10.1002/2013GL057705.

Jähne, B., G. Heinz, and W. Dietrich (1987), Measurement of the diffusion coefficients of sparingly soluble gases in water, *J. Geophys. Res., 92*(C10), 10767–10776, doi:10.1029/JC092iC10p10767.

Jassal, R. S., T. A. Black, G. B. Drewitt, M. D. Novak, D. Gaumont-Guay, and Z. Nesic (2004), A model of the production and transport of CO_2 in soil: predicting soil CO_2 concentrations and CO_2 efflux from a forest floor, *Agricultural and Forest Meteorology, 124*(3-4), 219–236, doi:10.1016/j.agrformet.2004.01.013.

Johnson, M. S., M. F. Billett, K. J. Dinsmore, M. Wallin, K. E. Dyson, and R. S. Jassal (2010), Direct and continuous measurement of dissolved carbon dioxide in freshwater aquatic systems—Methods and applications, *Ecohydrology, 3*(1), 68–78, doi:10.1002/eco.95.

Jones, J. B., and P. J. Mulholland (1998), Influence of drainage basin topography and elevation on carbon dioxide and methane supersaturation of stream water, *Biogeochemistry, 40*(1), 57–72, doi:10.1023/A:1005914121280.

Jonsson, A., J. Aberg, A. Lindroth, and M. Jansson (2008), Gas transfer rate and CO2 flux between an unproductive lake and the atmosphere in northern Sweden, *J. Geophys. Res. Biogeosci., 113*, G4, doi:10.1029/2008JG000688

Kling, G. W., G. W. Kipphut, and M. C. Miller (1991), Arctic lakes and streams and gas conduits to the atmosphere: Implications for tundra carbon budgets, *Science, 251*(4991), 298–301, doi:10.1126/science.251.4991.298.

Kokic, J., M. B. Wallin, H. E. Chmiel, B. A. Denfeld, and S. Sobek (2015), Carbon dioxide evasion from headwater systems strongly contributes to the total export of carbon from a small boreal lake catchment, *J. Geophys. Res. Biogeosci., 120*, 13–28, doi:10.1002/2014JG002706.

Leach, J. A., and Moore, R. D. (2014). Winter stream temperature in the rain-on-snow zone of the Pacific Northwest: influences of hillslope runoff and transient snow cover. *Hydrology and Earth System Sciences, 18*(2), 819–838, doi:10.5194/hess-18-819-2014

Looman, A., I. R. Santos, D. R. Tait, J. R. Webb, C. A. Sullivan, and D. T. Maher (2016), Carbon cycling and exports over diel and flood-recovery timescales in a subtropical rainforest headwater stream, *Sci. Total Environ., 550*, 645–657.

MacIntyre, S., A. Jonsson, M. Jansson, J. Aberg, D. E. Turney, and S. D. Miller (2010), Buoyancy flux, turbulence, and the gas transfer coefficient in a stratified lake, *Geophys. Res. Lett., 37*(24), L24604, doi:10.1029/2010GL044164.

MacIntyre, S., R. Wanninkhof, and J. P. Chanton (1995), Trace gas exchange across the air-water interface in freshwater and coastal marine environments, in *Biogenic Trace Gases: Measuring Emissions From Soil and Water*, edited by P. A. Matson and R. C. Harriss, 52–97.

Marx, A., et al, (2017), A review of CO_2 and associated carbon dynamics in headwater streams: a global perspective, *Reviews of Geophysics*, doi:10.1002/2016RG000547

Marzolf, E. R., P. J. Mulholland, and A. D. Steinman, (1994), Improvements to the diurnal upstream-downstream dissolved oxygen change technique for determining whole-stream metabolism in small streams. *Can. J. Fish. Aquat. Sci. 51*(7), 1591–1599, doi:10.1139/f94-158.

McClain, M. E., et al. (2003), Biogeochemical hot spots and hot moments at the interface of terrestrial and aquatic ecosystems, *Ecosystems, 6*(4), 301–312, doi: 10.1007/s10021-003-0161-9

Melching, C. S., and H. E. Flores (1999), Reaeration equations derived from US Geological Survey database, *J. Environ. Eng., 125*, 407–414, doi:10.1061/(ASCE)0733-9372(1999)125:5(407).

Moog, D. B., and G. H. Jirka (1999), Stream reaeration in nonuniform flow: Macroroughness enhancement. *J. Hydraul. Eng., 125*(1), 11–16, doi:10.1061/(ASCE)0733-9429(1999)125:1(11).

Moore, R. D. (2005), Slug injection using salt in solution, *Streamline Watershed Management Bulletin*, *8*(2), 1-6.

Mulholland, P. J., et al., (2001), Inter-biome comparison of factors controlling stream metabolism. *Freshw. Biol. 46*(11), 1503–1517, doi:10.1046/j.1365-2427.2001.00773.x.

Natchimuthu, S., M. B. Wallin, L. Klemedtsson, and D. Bastviken (2017), Spatio-temporal patterns of stream methane and carbon dioxide emissions in a hemiboreal catchment in Southwest Sweden, *Sci. Rep., 7*, 39729, doi:10.1038/srep39729.

O'Connor, D., and W. Dobbins (1958), Mechanism of reaeration in natural streams, *Trans. Am. Soc. Civ. Eng. 123*(1), 641–666.

Öquist, M. G., M. Wallin, J. Seibert, K. Bishop, and H. Laudon (2009), Dissolved inorganic carbon export across the soil/stream interface and its fate in a boreal headwater stream, *Environ. Sci. Technol., 43*(19), 7364–7369, doi:10.1021/es900416h.

Plummer, L. N., and E. Busenberg (1982), The Solubilities of Calcite, Aragonite and Vaterite in CO_2-H_2O Solutions between 0 and 90°C, and an Evaluation of the Aqueous Model for the System $CaCO_3$-CO_2-H_2O, *Geochim. Cosmochim. Ac., 46*(6), 1011-1040, doi:10.1016/0016-7037(82)90056-4

R Core Team (2017). R: A language and environment for statistical computing. R Foundation for Statistical Computing, Vienna, Austria. URL https://www.R-project.org/.

Raymond, P. A., and J. J. Cole (2001), Gas exchange in rivers and estuaries: Choosing a gas transfer velocity, *Estuaries, 24*(2), 312–317, doi:10.2307/1352954.

Raymond, P. A., C. J. Zappa, D. Butman, T. L. Bott, J. Potter, P. Mulholland, A. E. Laursen, W. H. McDowell, and D. Newbold (2012), Scaling the gas transfer velocity and hydraulic geometry in streams and small rivers, *Limnol. Oceanogr. Fluids Environ., 2*(1), 41–53, doi:10.1215/21573689-1597669.

Raymond, P. A., et al. (2013), Global carbon dioxide emissions from inland waters, *Nature, 503*(7476), 355–359, doi:10.1038/nature12760.

Richardson, J. S., and R. D. Moore (2010), Malcolm Knapp Research Forest, *Streamline Watershed Management Bulletin 14*(1), 14–15.

Richardson, M. E., G. Sentlinge, D. Moore, and A. Zimmermann (2017), Quantifying the Relation between Electrical Conductivity and Salt Concentration for Dilution Gauging Via Dry Salt Injection, *Confluence: Journal of Watershed Science and Management, 1*(2), 1–13, doi:10.22230/jwsm.2017v1n1a1.

Roberts, B. J., P. J. Mulholland, and W. R. Hill (2007), Multiple scales of temporal variability in ecosystem metabolism rates: Results from 2 years of continuous monitoring in a forested headwater stream, *Ecosystems 10*(4), 588–606, doi:10.1007/s10021-007-9059-2.

Sand-Jensen, K., and P. A. Staehr (2012), CO_2 dynamics along Danish lowland streams: water-air gradients, piston velocities, and evasion rates, *Biogeochemistry, 111*(1-3), 615–628, doi: 10.1007/s10533-011-9696-6.

Sawakuchi, H. O., et al. (2017), Carbon Dioxide Emissions along the Lower Amazon River, *Front. Mar. Sci., 4*, 76, doi:10.3389/fmars.2017.00076.

Schelker, J., G. A. Singer, A. J. Ulseth, S. Hengsberger, T. J. Battin (2016), CO_2 evasion from a steep, high gradient stream network: importance of seasonal and diurnal variation in aquatic pCO_2 and gas transfer, *Limnol. Oceanogr., 61*(5), 1826–1838, doi: 10.1002/lno.10339.

Schindler, J. E., and D. P. Krabbenhoft (1998), The hyporheic zone as a source of dissolved organic carbon and carbon gases to a temperate forested stream, *Biogeochemistry 43*(2), 157–174.

Shaw, E. M., K. J. Beven, N. A. Chappell, and R. Lamb (2010), *Hydrology in practice*, 4th edn. CRC Press, Boca Raton.

Simonsen, J.F. (1974), Oxygen fluctuations in streams, Ph.D. thesis, Danish Technical University, Copenhagen.

Smits, A. P. (2016), Physical controls on land-water linkages: Carbon cycling and food webs in boreal watersheds, Ph.D. thesis, University of Washington, Seattle.

Stackpoole S, et al., (2012), Baseline carbon sequestration, transport, and emission from inland aquatic ecosystems in the western United States. Baseline and Projected Future Carbon Storage and Greenhouse-Gas Fluxes in Ecosystems of the Western United States, *US Geological Survey Professional Paper*, 1797, eds Z. Zhu, and B. C. Reed.

Stackpoole, S. M., D. E. Butman, D. W. Clow, K. L. Verdin, B. V. Gaglioti, H. Genet, and R. G. Striegl (2017), Inland waters and their role in the carbon cycle of Alaska. *Ecological Applications, 27*(5), 1403–1420, doi: 10.1002/eap.1552.

Tashe, N.C., (1998), The impact of vine maple on the biogeochemical nutrient cycle of conifer-dominated coastal forests in southwestern British Columbia, M.Sc. thesis, Simon Fraser University, Burnaby, British Columbia.

Thyssen, N., and M. G. Kelly (1985), Water-air exchange of carbon dioxide and oxygen in a river: measurement and comparison of rates, *Arch. Hydrobiol. 105*(2), 219–228.

Tobias, C. R., J. K. Böhlke, J. W. Harvey, and E. Busenberg (2009), A simple technique for continuous measurement of time-variable gas transfer in surface waters, *Limnol. Oceanogr.: Methods, 7*(2), 185–195, doi:10.4319/lom.2009.7.185.

Tsivoglou, E. C., and R. J. Wallace (1972), Characterization of Stream Reaeration Capacity, *Research Reporting Series*, U.S. Environmental Protection Agency, 317.

Tsivoglou, E. C., and A. L. Neal (1976), Tracer measurement of reaeration, III: Predicting reaeration capacity of inland streams, *J. Water Pollut. Control Fed., 48*(12), 2669–2689.

Turk, T. D., M. G. Schmidt, and N. J. Roberts, (2008), The influence of bigleaf maple on forest floor and mineral soil properties in a coniferous forest in coastal British Columbia, *Forest Ecology and Management, 255*(5), 1874-1882.

Vachon, D., Y. T. Prairie, and J. J. Cole (2010), The relationship between near-surface turbulence and gas transfer velocity in freshwater systems and its implications for floating chamber measurements of gas exchange, *Limnol. Oceanogr., 55*(4), 1723–1732, doi:10.4319/lo.2010.55.4.1723.

Waldon, M. G. (2004), Estimation of average stream velocity, *J. Hydraul. Eng., 130*(11), 1119–1122, doi:10.1061/(ASCE)0733-9429(2004)130.11(1119).

Wallin, M. B., T. Grabs, I. Buffam, H. Laudon, A. Agren, M. G. Öquist, K. Bishop (2013), Evasion of CO_2 from streams – The dominant component of the carbon export through the aquatic conduit in a boreal landscape, *Global Change Biology, 19*(3), 785–797, doi:10.1111/gcb.12083.

Wallin, M. B., M. G. Öquist, I. Buffam, M. F. Billett, J. Nisell, and K. H. Bishop (2011), Spatiotemporal variability of the gas transfer coefficient K(CO_2) in boreal streams: Implications for large scale estimates of CO_2 evasion, *Global Biogeochem. Cycles, 25*(14), Gb3025, doi:10.1029/ 2010gb003975.

Wanninkhof, R., Mulholland, P. J., and Elwood, J. W. (1990), Gas exchange rates for a first-order stream determined with deliberate and natural tracers, *Water Resources Research*, *26*(7), 1621–1630, http://doi.org/10.1029/WR026i007p01621.

Wanninkhof, R., W. E. Asher, D. T. Ho, C. Sweeney, and W. R. McGillis (2009), Advances in Quantifying Air-Sea Gas Exchange and Environmental Forcing, *Annu. Rev. Mar. Sci.*, *1*, 213-244, doi:10.1146/annurev.marine.010908.163742.

Zappa, C. J., W. R. McGillis, P. A. Raymond, J. B. Edson, E. J. Hintsa, H. J. Zemmelink, J. W. H. Dacey, and D. T. Ho (2007), Environmental turbulent mixing controls on air-water gas exchange in marine and aquatic systems, *Geophys. Res. Lett.*, *34*(10), L10601, doi:10.1029/2006GL028790.

Appendix 1

CR1000 program used for autonomous and unaccompanied measurement

```
'Program for WQ and Vaisala sensors
'date edited: October 14, 2016
'author: mollie

'====== VARIABLES ================================

'general
Public PTemp, batt_volt
Units PTemp = Deg C
Units batt_volt = Volts

Public lowPowerMode
Public MinBattVolt
Public powerPhone
Public phoneManualON
Public firstDataWindow, secondDataWindow

'time
Public real_time(9)
Alias real_time(1) = year
Alias real_time(2) = month
Alias real_time(3) = DayX
Alias real_time(4) = hours
Alias real_time(5) = minutes
Alias real_time(6) = seconds
Alias real_time(7) = microseconds
Alias real_time(8) = weekday
Alias real_time(9) = jday
'Public mins_current_day

'constants
Const port_phone_power = 6
Const port_AM32B_CLK = 1
Const port_AM32B_RES = 2
Const port_SV_power = 7
Const port_CO2_power = 8

'Solenoid valve
Public powerSV

'Vaisala CO2 variables
```

```
Public CO2_1_mV, CO2_1_ppm, CO2_2_mV, CO2_2_ppm, measureCO2, powerCO2, measureCO2_30, powerCO2_30

'CTD variables
Public CTD_1(3), CTD_2(3)
Alias CTD_1(1) = Depth_CTD_1
Alias CTD_1(2) = Temp_CTD_1
Alias CTD_1(3) = EC_CTD_1
Alias CTD_2(1) = Depth_CTD_2
Alias CTD_2(2) = Temp_CTD_2
Alias CTD_2(3) = EC_CTD_2

Units Depth_CTD_1 = mm
Units Temp_CTD_1 = Deg C
Units EC_CTD_1 = uS/m
Units Depth_CTD_2 = mm
Units Temp_CTD_2 = Deg C
Units EC_CTD_2 = uS/m

'pH/ORP variables
Public pH_1, pH_2, ORP_1
Dim pHMult_1, pHMult_2

Units pH_1 = pH
Units pH_2 = pH
Units ORP_1 = mV

'DO variables
Public Tw_LDO, LDO

'GS3 variables
Public GS3_1(3), GS3_2(3)
Alias GS3_1(1) = Moisture_GS3_1
Alias GS3_1(2) = Temp_GS3_1
Alias GS3_1(3) = EC_GS3_1
Alias GS3_2(1) = Moisture_GS3_2
Alias GS3_2(2) = Temp_GS3_2
Alias GS3_2(3) = EC_GS3_2

'anemometer variables
Public u, v, w, SonicT
Units u = ms-1
Units v = ms-1
Units w = ms-1
Units SonicT = DegC
```

```
'======== Data tables ============================
'30 minute table
DataTable(dt,true,-1)
  DataInterval(0,30,Min,10)
  Average(1,batt_volt,FP2,0)
  Average(1,PTemp,FP2,0)
  Average(1,CO2_1_ppm,IEEE4,measureCO2_30-1) 'this makes it track the data only if "measureCO2_30" = true
  Average(1,CO2_2_ppm,IEEE4,measureCO2_30-1)
  Average(3,CTD_1(),IEEE4,0)
  Average(3,CTD_2(),IEEE4,0)
  Average(1,ORP_1,IEEE4,0)
  Average(1,pH_1,IEEE4,0)
  Average(1,pH_2,IEEE4,0)
  Average(1,LDO, IEEE4,0)
  Average(1,Tw_LDO,IEEE4,0)
  Average(3,GS3_1(),IEEE4,0)
  Average(3,GS3_2(),IEEE4,0)
  Average(1,u,IEEE4,0)
  Average(1,v,IEEE4,0)
  Average(1,w,IEEE4,0)
  Average(1,SonicT,IEEE4,0)
EndTable

'5 second table - only activated when measureCO2 = true
DataTable(dt_co2,true,-1)
  DataInterval(0,5,Sec,10)
  Average(1,CO2_1_ppm,IEEE4,measureCO2-1) 'this makes it track the data only if "measureCO2" = true
  Average(1,CO2_2_ppm,IEEE4,measureCO2-1)
  Average(3,CTD_1(),IEEE4,0)
  Average(3,CTD_2(),IEEE4,0)
  Average(1,ORP_1,IEEE4,0)
  Average(1,pH_1,IEEE4,0)
  Average(1,pH_2,IEEE4,0)
  Average(1,LDO, IEEE4,0)
  Average(1,Tw_LDO,IEEE4,0)
  Average(3,GS3_1(),IEEE4,0)
  Average(3,GS3_2(),IEEE4,0)
  Average(1,u,IEEE4,0)
  Average(1,v,IEEE4,0)
  Average(1,w,IEEE4,0)
  Average(1,SonicT,IEEE4,0)
EndTable

'Main Program
```

```
BeginProg
  firstDataWindow  =  15
  secondDataWindow =  16
  phoneManualON = 0
  MinBattVolt = 11.4

Scan (5,Sec,0,0)

'======== Panel Temp/Battery ============================
            PanelTemp (PTemp,250)
                    Battery (batt_volt)
    RealTime real_time

'====== Low power mode ====================
    If batt_volt < MinBattVolt Then
      lowPowerMode = 1
    Else
      lowPowerMode = 0
    EndIf

'======== SDI: CTD/GS3 ============================
  'CTD measurements
    Delay (1,200,mSec)
    SDI12Recorder (CTD_1(),3,1,"M!",1.0,0)
    Delay (1,200,mSec)
    SDI12Recorder (CTD_2(),3,6,"M!",1.0,0)

  'GS3 measurements
    Delay (1,200,mSec)
    SDI12Recorder (GS3_1(),3,3,"M!",1.0,0)
    Delay (1,200,mSec)
    SDI12Recorder (GS3_2(),5,4,"M!",1.0,0)

'======== Solenoid and CO2 ============================
  'SV switch - change to reflect how long to inject CO2
    If (hours = 10 OR hours = 22) AND NOT lowPowerMode Then 'AND (minutes >= 0 AND
minutes <= 59)
      powerSV = 1
    Else
      powerSV = 0
    EndIf
    PortSet(port_SV_power,powerSV)

          'CO2 ppm measurements - on or off
             If (hours = 10 OR hours = 22) AND NOT lowPowerMode Then ' AND (minutes <=
59))
```

```
    powerCO2 = 1
  Else
    powerCO2 = 0
  EndIf

' Put CO2 on 30 min output table
        'CO2 ppm measurements - on or off
         If ((minutes >= 25) AND (minutes <= 30)) OR ((minutes >= 55) AND (minutes <=
60)) AND NOT lowPowerMode Then
    powerCO2_30 = 1
  Else
    powerCO2_30 = powerCO2
  EndIf

 If powerCO2_30 = 1 Then
    powerCO2 = 1
 EndIf

  PortSet(port_CO2_power,powerCO2)


  If powerCO2 AND (hours = 10 OR hours = 22) Then 'AND (minutes <= 59))
    measureCO2 = 1
  Else
    measureCO2 = 0
  EndIf

  If powerCO2_30 AND (((minutes >= 28) AND (minutes <= 30)) OR ((minutes >= 58) AND
(minutes <= 60))) Then
    measureCO2_30 = 1
  Else
    measureCO2_30 = 0
  EndIf

'======== PHONE ============================
 ' Turn the phone on for one hour during the first time window
 ' (uncomment 'OR' and remove the 1st 'Then' to turn on for 30 mins during each of two time
windows
 If (hours = firstDataWindow)  AND NOT lowPowerMode Then 'OR hours =
secondDataWindow) AND minutes < 30 Then
  powerPhone = 1
 Else
  powerPhone = 0
 EndIf
 ' Use the phoneManualON flag to keep the phone on forever
 ' the default value for phoneManualON will be 0 (OFF)
```

```
  If phoneManualON = 1  AND NOT lowPowerMode Then
    powerPhone = 1
  EndIf
  PortSet(port_phone_power,powerPhone)
  '-----------------------------------------

'======== Multiplexer: pH, ORP, DO, CO2 ============================
  'multiplexer ON
    PortSet(port_AM32B_RES,1)

  'pH measurements - see WQ program for cal slope lines
  'change temp variable to GS3 if that's better
    PulsePort (port_AM32B_CLK,10000) ' move to the next channel of AM32B
    pHMult_1=-1/(((Temp_CTD_1+273)/298)*59)
    VoltDiff(pH_1,1,mV2500,1,True,0,_60Hz,pHMult_1,7)

    PulsePort (port_AM32B_CLK,10000)
    pHMult_2=-1/(((Temp_CTD_2+273)/298)*59)
    VoltDiff(pH_2,1,mV2500,2,True,0,_60Hz,pHMult_2,7)

  'ORP measurements
    PulsePort (port_AM32B_CLK,10000) ' move to the next channel of AM32B
    VoltDiff(ORP_1,1,mV2500,1,True,0,_60Hz,1,0)

  'DO measurements
    PulsePort (port_AM32B_CLK,10000) ' move to the next channel of AM32B
    VoltDiff (LDO,1,mV2500,1,True,0,_60Hz,0.02,0)
    VoltDiff (Tw_LDO,1,mV2500,2,True,0,_60Hz,0.05,0)

  'vaisala CO2 measurements
    PulsePort (port_AM32B_CLK,10000) ' move to the next channel of AM32B
                VoltDiff (CO2_1_mV,1,mV2500,1,True,0,250,1.0,0)
                CO2_1_ppm = CO2_1_mV * 4
                VoltDiff (CO2_2_mV,1,mV2500,2,True,0,250,1.0,0)
                CO2_2_ppm = CO2_2_mV * 4

  'end multiplexer
    PortSet(port_AM32B_RES,0)

'======== Diff Channels on CR1000: Sonic ============================

  'sonic measurements
    VoltDiff (u,1,mV5000,5,True ,0,250,1.0,0)
    u = ((25*2/5000)*u)-25
    VoltDiff (v,1,mV5000,6,True ,0,250,1.0,0)
    v = ((25*2/5000)*v)-25
```

```
    VoltDiff (w,1,mV5000,7,True ,0,250,1.0,0)
    w = ((25*2/5000)*w)-25
    VoltDiff (SonicT,1,mV5000,8,True ,0,250,1.0,0)
    SonicT = ((100/5000)*SonicT)+220-273.15

'======== Call data tables ============================
  CallTable(dt)
  If measureCO2 = 1 Then
    CallTable(dt_co2)
  EndIf

        NextScan
EndProg
```

Appendix 2

CR1000 program used for autonomous and accompanied measurement

```
'Program for WQ and Vaisala sensors
'date edited: October 14, 2016
'author: mollie

'====== VARIABLES ================================

'general
Public PTemp, batt_volt
Units PTemp = Deg C
Units batt_volt = Volts

Public lowPowerMode
Public MinBattVolt
Public powerPhone
Public phoneManualON
Public firstDataWindow, secondDataWindow

'time
Public real_time(9)
Alias real_time(1) = year
Alias real_time(2) = month
Alias real_time(3) = DayX
Alias real_time(4) = hours
Alias real_time(5) = minutes
Alias real_time(6) = seconds
Alias real_time(7) = microseconds
Alias real_time(8) = weekday
Alias real_time(9) = jday
'Public mins_current_day

'constants
Const port_phone_power = 6
Const port_AM32B_CLK = 1
Const port_AM32B_RES = 2
Const port_SV_power = 7
Const port_CO2_power = 8

'Solenoid valve
'Public powerSV

'Vaisala CO2 variables
Public CO2_1_mV, CO2_1_ppm, CO2_2_mV, CO2_2_ppm, measureCO2, powerCO2
```

```
'CTD variables
Public CTD_1(3), CTD_2(3)
Alias CTD_1(1) = Depth_CTD_1
Alias CTD_1(2) = Temp_CTD_1
Alias CTD_1(3) = EC_CTD_1
Alias CTD_2(1) = Depth_CTD_2
Alias CTD_2(2) = Temp_CTD_2
Alias CTD_2(3) = EC_CTD_2

Units Depth_CTD_1 = mm
Units Temp_CTD_1 = Deg C
Units EC_CTD_1 = uS/m
Units Depth_CTD_2 = mm
Units Temp_CTD_2 = Deg C
Units EC_CTD_2 = uS/m

'pH/ORP variables
Public pH_1, pH_2, ORP_1
Dim pHMult_1, pHMult_2

Units pH_1 = pH
Units pH_2 = pH
Units ORP_1 = mV

'DO variables
Public Tw_LDO, LDO

'GS3 variables
Public GS3_1(3), GS3_2(3)
Alias GS3_1(1) = Moisture_GS3_1
Alias GS3_1(2) = Temp_GS3_1
Alias GS3_1(3) = EC_GS3_1
Alias GS3_2(1) = Moisture_GS3_2
Alias GS3_2(2) = Temp_GS3_2
Alias GS3_2(3) = EC_GS3_2

'anemometer variables
Public u, v, w, SonicT
Units u = ms-1
Units v = ms-1
Units w = ms-1
Units SonicT = DegC

'======== Data tables ============================
'30 minute table
```

```
DataTable(dt_co2on,true,-1)
  DataInterval(0,30,Min,10)
  Average(1,batt_volt,FP2,0)
  Average(1,PTemp,FP2,0)
  Average(1,CO2_1_ppm,IEEE4,measureCO2-1) 'this makes it track the data only if
"measureCO2" = true
  Average(1,CO2_2_ppm,IEEE4,measureCO2-1)
  Average(3,CTD_1(),IEEE4,0)
  Average(3,CTD_2(),IEEE4,0)
  Average(1,ORP_1,IEEE4,0)
  Average(1,pH_1,IEEE4,0)
  Average(1,pH_2,IEEE4,0)
  Average(1,LDO, IEEE4,0)
  Average(1,Tw_LDO,IEEE4,0)
  Average(3,GS3_1(),IEEE4,0)
  Average(3,GS3_2(),IEEE4,0)
  Average(1,u,IEEE4,0)
  Average(1,v,IEEE4,0)
  Average(1,w,IEEE4,0)
  Average(1,SonicT,IEEE4,0)
EndTable

'5 second table - only activated when measureCO2 = true
DataTable(dt_co2_co2on,true,-1)
  DataInterval(0,5,Sec,10)
  Average(1,CO2_1_ppm,IEEE4,measureCO2-1) 'this makes it track the data only if
"measureCO2" = true
  Average(1,CO2_2_ppm,IEEE4,measureCO2-1)
  Average(3,CTD_1(),IEEE4,0)
  Average(3,CTD_2(),IEEE4,0)
  Average(1,ORP_1,IEEE4,0)
  Average(1,pH_1,IEEE4,0)
  Average(1,pH_2,IEEE4,0)
  Average(1,LDO, IEEE4,0)
  Average(1,Tw_LDO,IEEE4,0)
  Average(3,GS3_1(),IEEE4,0)
  Average(3,GS3_2(),IEEE4,0)
  Average(1,u,IEEE4,0)
  Average(1,v,IEEE4,0)
  Average(1,w,IEEE4,0)
  Average(1,SonicT,IEEE4,0)
EndTable

'Main Program
BeginProg
   PortsConfig (&B11111111,&B11111111)
```

```
  firstDataWindow  =  15
  secondDataWindow =  16
  phoneManualON = 0
  MinBattVolt = 11.4

Scan (5,Sec,0,0)

'======== Panel Temp/Battery ============================
            PanelTemp (PTemp,250)
                    Battery (batt_volt)

    RealTime real_time


'====== Low power mode ====================
    If batt_volt < MinBattVolt Then
      lowPowerMode = 1
    Else
      lowPowerMode = 0
    EndIf


'======== SDI: CTD/GS3 ============================
  'CTD measurements
    Delay (1,200,mSec)
    SDI12Recorder (CTD_1(),3,1,"M!",1.0,0)
    Delay (1,200,mSec)
    SDI12Recorder (CTD_2(),3,6,"M!",1.0,0)

  'GS3 measurements
    Delay (1,200,mSec)
    SDI12Recorder (GS3_1(),3,3,"M!",1.0,0)
    Delay (1,200,mSec)
    SDI12Recorder (GS3_2(),5,4,"M!",1.0,0)

'======== Solenoid and CO2 ============================
  'SV switch - change to reflect how long to inject CO2
   ' If ((minutes >= 25 AND minutes < 30) OR (minutes >= 55)) AND NOT lowPowerMode
Then
    'powerSV = 1
    'Else
     ' powerSV = 0
    'EndIf
    'PortSet(port_SV_power,powerSV)

          'CO2 ppm measurements - on or off
```

```
          '  If ((minutes >= 23 AND minutes < 30) OR (minutes >= 53)) AND NOT
lowPowerMode Then
     powerCO2 = 1
  '  Else
    '  powerCO2 = 0
   ' EndIf

    PortSet(port_CO2_power,powerCO2)

  '  If powerCO2 AND ((minutes >= 25 AND minutes < 30) OR (minutes >= 55)) Then
      measureCO2 = 1
  '  Else
   '   measureCO2 = 0
  '  EndIf

'======== PHONE ============================
  ' Turn the phone on for one hour during the first time window
  ' (uncomment 'OR' and remove the 1st 'Then' to turn on for 30 mins during each of two time
windows
  If (hours = firstDataWindow)  AND NOT lowPowerMode Then 'OR hours =
secondDataWindow) AND minutes < 30 Then
    powerPhone = 1
  Else
    powerPhone = 0
  EndIf
  ' Use the phoneManualON flag to keep the phone on forever
  ' the default value for phoneManualON will be 0 (OFF)
  'If phoneManualON = 1  AND NOT lowPowerMode Then
    'powerPhone = 1
  'EndIf
  PortSet(port_phone_power,powerPhone)
  '-----------------------------------------

'======== Multiplexer: pH, ORP, DO, CO2 ============================
  'multiplexer ON
    PortSet(port_AM32B_RES,1)

  'pH measurements - see WQ program for cal slope lines
  'change temp variable to GS3 if that's better
    PulsePort (port_AM32B_CLK,10000) ' move to the next channel of AM32B
    pHMult_1=-1/(((Temp_CTD_1+273)/298)*59)
    VoltDiff(pH_1,1,mV2500,1,True,0,_60Hz,pHMult_1,7)

    PulsePort (port_AM32B_CLK,10000)
    pHMult_2=-1/(((Temp_CTD_2+273)/298)*59)
    VoltDiff(pH_2,1,mV2500,2,True,0,_60Hz,pHMult_2,7)
```

```
  'ORP measurements
    PulsePort (port_AM32B_CLK,10000) ' move to the next channel of AM32B
    VoltDiff(ORP_1,1,mV2500,1,True,0,_60Hz,1,0)

  'DO measurements
    PulsePort (port_AM32B_CLK,10000) ' move to the next channel of AM32B
    VoltDiff (LDO,1,mV2500,1,True,0,_60Hz,0.02,0)
    VoltDiff (Tw_LDO,1,mV2500,2,True,0,_60Hz,0.05,0)

  'vaisala CO2 measurements
    PulsePort (port_AM32B_CLK,10000) ' move to the next channel of AM32B
                VoltDiff (CO2_1_mV,1,mV2500,1,True,0,250,1.0,0)
                CO2_1_ppm = CO2_1_mV * 4
                VoltDiff (CO2_2_mV,1,mV2500,2,True,0,250,1.0,0)
                CO2_2_ppm = CO2_2_mV * 4

  'end multiplexer
    PortSet(port_AM32B_RES,0)

'======== Diff Channels on CR1000: Sonic ============================

  'sonic measurements
    VoltDiff (u,1,mV5000,5,True ,0,250,1.0,0)
    u = ((25*2/5000)*u)-25
    VoltDiff (v,1,mV5000,6,True ,0,250,1.0,0)
    v = ((25*2/5000)*v)-25
    VoltDiff (w,1,mV5000,7,True ,0,250,1.0,0)
    w = ((25*2/5000)*w)-25
    VoltDiff (SonicT,1,mV5000,8,True ,0,250,1.0,0)
    SonicT = ((100/5000)*SonicT)+220-273.15

'======== Call data tables ============================
  CallTable(dt_co2on)
  CallTable(dt_co2_co2on)

        NextScan
EndProg
```

Appendix 3

Description of headspace analysis via gas chromatography

I collected air samples from above the stream reach in duplicate for analysis on a gas chromatograph (Agilent 7890A GC system) and calculation of atmospheric CO_2. In this method, I collected 30 mL of air in a syringe, attach a filter with a needle to the syringe, and inject the air into a sealed vial for analysis. I repeated this on multiple occasions during the study period to determine the average atmospheric CO_2 concentration at the study site. This parameter is used in calculations of k_{CO2}, k_{600}, and CO_2 emissions.

Appendix 4

Input stream velocity (V) (m s^{-1}) and the logarithm of predicted CO_2 emissions estimates ($log(F_{CO2})$) (g C L^{-1} d^{-1}) of the loess fit

V	$log(F_{CO2})$
0.22	4.11
0.27	4.74
0.36	6.01
0.25	4.53
0.21	4.08
0.16	3.59
0.25	4.49
0.23	4.22
0.23	4.28
0.30	5.06
0.26	4.60
0.21	3.99
0.18	3.73
0.16	3.60
0.15	3.50
0.22	4.14
0.30	5.13
0.34	5.66
0.25	4.52
0.23	4.20

0.24	4.32
0.23	4.24
0.33	5.54
0.29	4.99
0.24	4.31
0.20	3.93
0.17	3.68
0.15	3.53
0.14	3.43
0.14	3.44
0.21	4.08
0.26	4.55
0.21	4.04
0.18	3.76
0.16	3.60
0.14	3.47
0.13	3.38
0.12	3.32
0.13	3.38
0.15	3.52
0.15	3.54
0.15	3.51
0.17	3.71
0.18	3.74
0.11	3.25

0.11	3.22
0.09	3.12
0.07	3.06
0.06	3.02
0.05	3.01
0.05	3.01
0.08	3.07
0.07	3.04
0.05	3.01
0.05	2.99
0.04	2.98
0.08	3.09
0.07	3.07
0.06	3.02
0.05	3.00
0.04	2.98
0.13	3.38
0.27	4.77
0.20	3.93
0.14	3.47
0.12	3.29
0.10	3.20
0.21	4.03
0.32	5.39
0.11	3.26

0.10	3.21
0.09	3.14
0.08	3.11
0.07	3.07
0.07	3.06
0.07	3.04
0.06	3.02
0.06	3.03
0.08	3.10
0.22	4.19
0.31	5.25
0.20	3.95
0.16	3.61
0.14	3.45
0.15	3.48
0.19	3.85
0.29	5.03
0.30	5.14
0.35	5.76
0.32	5.34
0.26	4.60
0.31	5.26
0.23	4.30
0.19	3.84
0.23	4.22

0.22	4.17
0.17	3.66
0.14	3.42
0.12	3.31
0.11	3.23
0.12	3.28
0.13	3.39
0.12	3.31
0.14	3.47
0.23	4.30
0.31	5.17
0.20	3.94
0.17	3.69
0.17	3.68
0.14	3.44
0.12	3.29
0.12	3.33
0.15	3.52
0.15	3.52
0.16	3.56
0.22	4.11
0.20	3.94
0.27	4.73
0.23	4.28
0.23	4.27

0.25	4.52
0.23	4.31
0.22	4.11
0.19	3.83
0.18	3.74
0.14	3.43
0.12	3.32
0.10	3.22
0.20	3.95
0.30	5.12
0.23	4.21
0.18	3.74
0.16	3.56
0.14	3.46
0.12	3.29
0.12	3.34
0.11	3.27
0.12	3.28
0.13	3.36
0.18	3.77
0.16	3.61
0.19	3.87
0.16	3.61
0.13	3.39
0.11	3.25

0.09	3.15
0.10	3.18
0.18	3.73
0.21	4.00
0.17	3.67
0.15	3.49
0.23	4.22
0.22	4.12
0.17	3.65
0.14	3.42
0.12	3.28
0.10	3.17
0.08	3.10
0.08	3.08
0.06	3.02
0.06	3.01
0.05	3.00
0.04	2.98
0.03	2.97
0.03	2.96
0.03	2.96
0.04	2.97
0.06	3.01
0.06	3.03
0.05	3.00

0.04	2.98
0.03	2.97
0.03	2.96
0.07	3.05
0.06	3.02
0.09	3.14
0.06	3.02
0.05	2.99
0.04	2.98
0.04	2.98
0.04	2.97
0.04	2.97
0.12	3.30
0.09	3.12
0.07	3.07
0.07	3.06
0.06	3.03
0.05	3.00
0.05	2.99
0.04	2.98
0.03	2.97
0.03	2.96
0.02	2.96
0.02	2.96